

# Two-Scale Spatial Deployment for Cost-Effective Wireless Networks via Cooperative IRSs and Movable Antennas

Ying Gao, Qingqing Wu, Ziyuan Zheng, Yanze Zhu, Wen Chen, Xin Lin, and Shanpu Shen

**Abstract**—This paper proposes a two-scale spatial deployment strategy to ensure reliable coverage for multiple target areas, integrating macroscopic intelligent reflecting surfaces (IRSs) and fine-grained movable antennas (MAs). Specifically, IRSs are selectively deployed from candidate sites to shape the propagation geometry, while MAs are locally repositioned among discretized locations to exploit small-scale channel variations. The objective is to minimize the total deployment cost of MAs and IRSs by jointly optimizing the IRS site selection, MA positions, transmit precoding, and IRS phase shifts, subject to the signal-to-noise ratio (SNR) requirements for all target areas. This leads to a challenging mixed-integer non-convex optimization problem that is intractable to solve directly. To address this, we first formulate an auxiliary problem to verify the feasibility. A penalty-based double-loop algorithm integrating alternating optimization and successive convex approximation (SCA) is developed to solve this feasibility issue, which is subsequently adapted to obtain a suboptimal solution for the original cost minimization problem. Finally, based on the obtained solution, we formulate an element refinement problem to further reduce the deployment cost, which is solved by a penalty-based SCA algorithm. Simulation results demonstrate that the proposed designs consistently outperform benchmarks relying on independent area planning or full IRS deployment in terms of cost-efficiency. Moreover, for cost minimization, MA architectures are preferable in large placement apertures, whereas fully populated FPA architectures excel in compact ones; for worst-case SNR maximization, MA architectures exhibit a lower cost threshold for feasibility, while FPA architectures can attain peak SNR at a lower total cost.

**Index Terms**—Intelligent reflecting surface, movable antenna, two-scale spatial deployment, cost minimization, beamforming optimization.

## I. INTRODUCTION

Multiple-input multiple-output (MIMO) technology serves as a cornerstone of modern wireless networks, leveraging spatial diversity to optimize spectral efficiency [1]. As the industry transitions from the fifth-generation (5G) to the sixth-generation (6G) era, the severe shortage of available spectrum has necessitated the deployment of ultra-massive antenna arrays at base stations (BSs) to unlock high degrees of spatial multiplexing [2]. However, while these large-scale systems offer unprecedented connectivity, they impose significant burdens in terms of hardware expenditure and operational

Y. Gao, Q. Wu, Z. Zheng, Y. Zhu, and W. Chen are with the Department of Electronic Engineering, Shanghai Jiao Tong University, Shanghai 201210, China (e-mail: ying-gao@sjtu.edu.cn; qingqingwu@sjtu.edu.cn; zhengziyuan2024@sjtu.edu.cn; yanzezhu@sjtu.edu.cn; wenchen@sjtu.edu.cn). X. Lin is with the Shanghai Institute of Satellite Engineering, Shanghai 201109, China (e-mail: scar07@sina.com). S. Shen is with the State Key Laboratory of Internet of Things for Smart City and the Department of Electrical and Computer Engineering, University of Macau, Macau, China (e-mail: shanpushen@um.edu.mo).

energy consumption. Consequently, developing solutions that balance superior performance with cost-effectiveness and low complexity has become a critical research priority [3].

Intelligent reflecting surface (IRS) has emerged as a pivotal enabler for green and cost-effective communications [4]. By manipulating incident waves via massive passive elements, the IRS proactively reconfigures the radio environment to suppress interference and enhance link reliability. Beyond their lightweight structure and flexible deployment capabilities, these devices offer a squared power gain that scales with the number of elements [4], [5]. This significant potential has sparked extensive research into integrating IRSs with modern wireless networks [6]–[12]. In particular, numerous studies have been devoted to optimizing IRS-assisted networks for eliminating coverage blind spots [13]–[18]. For instance, the authors of [13] considered the co-design of active and passive beamforming alongside the placement of an aerial IRS to improve the minimum signal-to-noise ratio (SNR) in a target area. In a different context, the work in [14] studied a static regulated IRS with distributed MIMO technology. By coordinating multiple access points, this architecture effectively utilizes spatial diversity to enhance wireless coverage. Additionally, the authors of [18] investigated the cost-effective deployment of multiple IRSs by jointly optimizing the site selection and physical parameters to satisfy a specific coverage rate requirement.

Despite the channel reconfiguration capabilities of IRSs, the transceiver architectures are traditionally constrained by fixed-position antenna (FPA) geometries. Due to the lack of flexibility, such static designs limit the exploitation of spatial diversity and remain vulnerable to deep fading [19]. To overcome this limitation, movable antenna (MA) technology [20], also known as fluid antenna [21], has been introduced to enable flexible mechanical position adjustment within a confined region. By actively reconstructing the local channel environment to harvest the spatial variation gain fully, MAs achieve superior spectral efficiency and interference mitigation with fewer radio frequency (RF) chains [20], [22], [23]. Motivated by these advantages, extensive research efforts have been devoted to applying MAs to diverse domains, including multiuser networks [24]–[26], interference channels [27], multicast transmission [28], physical layer security [29], cognitive radio [30], and wireless-powered communications [31].

While both IRS and MA technologies are promising candidates for next-generation networks, they operate on fundamentally different principles. An IRS serves as a passive array that reshapes the propagation environment through phase

adjustments and requires an external source for signal transmission. Conversely, an MA actively optimizes channel quality by mechanically maneuvering the antenna position within a confined region. These distinct characteristics create a natural synergy between the two paradigms. Specifically, the IRS is effective at establishing virtual links to illuminate coverage blind spots, while the MA excels at harvesting spatial diversity across the continuous field. Furthermore, the deployment of IRSs enriches the multipath components in the environment, and this enables MAs to exploit spatial channel variations more efficiently [32]. Recent studies confirm that integrating IRSs with MAs yields superior performance compared to conventional IRS-aided FPA systems [33]. Significant improvements have been reported in terms of outage probability [34], data throughput [35]–[37], physical layer security [38], and coverage performance [39].

Despite the potential revealed in prior studies, two fundamental limitations remain. First, existing research on IRS-aided MA systems typically assumes fixed IRS deployment locations. This overlooks the practical need for optimal site selection in real network planning. Second, regarding the dimensioning of active and passive hardware, the authors of [39] provided a preliminary analysis of the trade-off between the number of MAs and IRS elements. However, that study primarily investigated the worst-case SNR performance under a fixed total budget by evaluating discrete combinations of antenna and element counts. Such a simulation-based performance-maximization approach is inapplicable to the practical network planning problem where the goal is to satisfy strict quality-of-service (QoS) requirements with minimal expenditure. Since the optimal hardware scale is unknown *a priori* and coupled with deployment positions, relying on the exhaustive search of discrete configurations becomes computationally prohibitive and inefficient. Consequently, there is a lack of systematic strategies for cost-effective network planning that jointly optimize the deployment of hardware resources and the configuration of transmission parameters to guarantee service quality.

Motivated by the above discussions, we study the cost-effective coverage problem in an IRS-aided MA system, as shown in Fig. 1. This system comprises a BS with a reconfigurable number of MAs and a set of candidate locations for IRS deployment, serving multiple target areas blocked by obstacles. Our main contributions are summarized as follows:

- To the best of the authors' knowledge, this is the first work to study two-scale spatial deployment for cost-effective IRS-aided MA systems. We establish a novel optimization framework where macroscopic IRS site selection shapes propagation geometry and microscopic MA placement exploits local channel variations. Specifically, a cost minimization problem is formulated by jointly optimizing these spatial parameters together with transmit precoding and IRS phase shifts, subject to the SNR requirements of all target areas. The resulting formulation involves binary deployment decisions and non-convex variable coupling, leading to a mixed-integer non-convex program that is challenging to solve directly.
- We develop a hierarchical optimization framework to tackle the mixed-integer non-convexity and coupling hur-

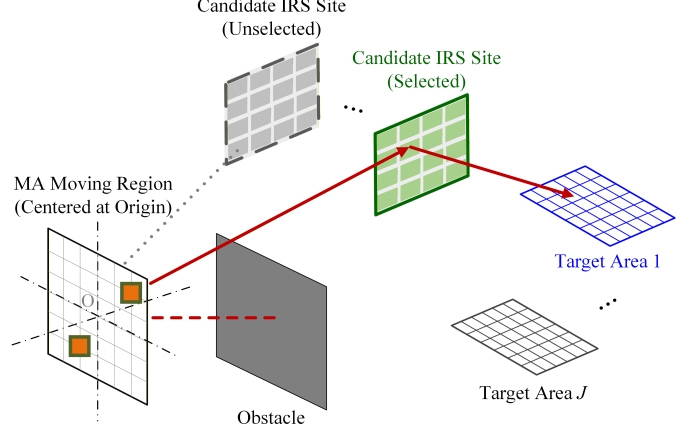


Fig. 1. Illustration of an IRS-aided MA system, involving joint IRS and MA deployment and configuration for cost-effective coverage.

dles. Specifically, a penalty-based double-loop algorithm integrating alternating optimization (AO) and successive convex approximation (SCA) is first designed to solve an auxiliary feasibility problem, ensuring a reliable initialization. This framework is then adapted for cost minimization, where the complex trilinear variable coupling is resolved via tight convex-hull linearization. Finally, an element-level refinement stage is introduced to prune hardware redundancy using a penalty-based SCA approach, further enhancing cost-efficiency while maintaining SNR guarantees.

- Numerical results show that: 1) A smaller MA step size improves feasibility with respect to the SNR constraints only when the resulting grid discretization preserves a non-decreasing maximum deployable antenna count  $M_{\max}$  under the minimum inter-MA distance constraint. 2) Compared with benchmarks based on independent area planning or full IRS activation, the proposed designs consistently achieve lower deployment costs. 3) Regarding cost minimization, MAs are superior in large placement apertures while FPAs with  $M_{\max}$  antennas suit compact ones; conversely, for worst-case SNR maximization, MAs offer a lower feasibility threshold, whereas such FPAs achieve peak performance at a lower total cost.

The remainder of this paper is organized as follows. Section II presents the system model and formulates the deployment cost minimization problem. Before solving the problem, Section III introduces a method to verify its feasibility. Section IV then proposes a computationally efficient algorithm to obtain a suboptimal solution of the problem. Building upon this, Section V refines the number of IRS elements to further reduce the deployment cost. Numerical results are presented in Section VI, followed by the conclusion in Section VII.

*Notations:* Let  $\mathbb{C}$  and  $\mathbb{C}^{M \times N}$  denote the set of complex numbers and the space of  $M \times N$  complex matrices, respectively. The superscripts  $(\cdot)^T$  and  $(\cdot)^H$  represent transpose and conjugate transpose, respectively. For any vector  $\mathbf{x}$ ,  $\|\mathbf{x}\|$  and  $[\mathbf{x}]_i$  denote its Euclidean norm and  $i$ -th entry, respectively. Similarly,  $[\mathbf{X}]_{i,j}$  denotes the  $(i, j)$ -th entry of matrix  $\mathbf{X}$ , and  $\mathbf{X}(:, m)$  denotes its  $m$ -th column. The operators  $\text{diag}(\cdot)$  and

`blkdiag`( $\cdot$ ) construct diagonal and block-diagonal matrices, respectively, while `Diag`( $\cdot$ ) extracts the main diagonal of a matrix as a vector. For a scalar  $x \in \mathbb{C}$ ,  $|x|$  and  $\Re\{x\}$  denote its magnitude and real component, with  $j^2 = -1$ .  $\mathbf{A} \succeq \mathbf{B}$  means  $\mathbf{A} - \mathbf{B}$  is positive semidefinite. Additionally,  $|\mathcal{K}|$  is the size of set  $\mathcal{K}$ , and  $\mathcal{CN}(\mu, \Sigma)$  denotes the circularly symmetric complex Gaussian distribution with mean vector  $\mu$  and covariance matrix  $\Sigma$ .  $\odot$  represents the Hadamard product.

## II. SYSTEM MODEL AND PROBLEM FORMULATION

### A. System Model

As shown in Fig. 1, we consider a downlink system providing area-wide coverage over  $J$  spatially separated target areas, indexed by  $\mathcal{J} \triangleq \{1, \dots, J\}$ . A BS is deployed at a remote location due to practical site planning constraints, such as site availability, land-lease cost, urban planning regulations, and backhaul access. Furthermore, severe terrestrial blockage obstructs the direct paths between the BS and target areas, rendering these links negligible. To address this connectivity issue, multiple passive IRSs are deployed at elevated positions to create virtual line-of-sight (LoS) links. We assume that there are  $L$  candidate sites available for IRS deployment, indexed by  $\mathcal{L} \triangleq \{1, \dots, L\}$ .

The BS is equipped with MAs connected to RF chains via flexible cables, enabling dynamic positioning within a square region  $\mathcal{C}$  of size  $A \times A$ . We adopt a three-dimensional (3D) Cartesian coordinate system with the BS reference point at the origin, where  $\mathcal{C}$  lies in the  $y$ - $z$  plane. Due to the fixed step size of electromechanical steppers, the antenna movement is quantized. The feasible MA locations are modeled as a discrete set of  $M$  grid points with coordinates  $\mathbf{t}_m \in \mathbb{R}^{3 \times 1}$  for  $m \in \mathcal{M} \triangleq \{1, \dots, M\}$ , arranged with a uniform step size of  $d$ . In the same coordinate system, a deployed IRS at candidate site  $\ell \in \mathcal{L}$  has element positions  $\{\mathbf{p}_{\ell,n}\}_{n=1}^{N_\ell} \subset \mathbb{R}^{3 \times 1}$ , with  $\mathbf{p}_{\ell,1}$  serving as the reference point. Furthermore, let  $\mathcal{A}_j \subset \mathbb{R}^{3 \times 1}$  denote the  $j$ -th target area and  $\mathbf{u}_j \in \mathcal{A}_j$  denote an arbitrary location in that area.

The  $J$  target areas are served sequentially, following either a round-robin cycle or a predetermined schedule. Accordingly, we define a binary variable  $x_{m,j} \in \{0, 1\}$  to indicate whether candidate location  $m$  is occupied by an MA when serving area  $j$  ( $x_{m,j} = 1$  if occupied and 0 otherwise). The MA configuration is area-adaptive, i.e.,  $x_{m,j}$  may differ from  $x_{m,j'}$  for  $j \neq j'$ . To enforce a minimum inter-MA separation, we impose the following constraint:

$$x_{m,j} + x_{q,j} \leq 1, \quad \forall (m, q) \in \mathcal{D}, j \in \mathcal{J}, \quad (1)$$

where the distance-based conflict set  $\mathcal{D}$  is defined as  $\mathcal{D} \triangleq \{(m, q) | m < q, \|\mathbf{t}_m - \mathbf{t}_q\| < D\}$ . This constraint ensures that no two MAs are simultaneously deployed at locations whose distance is smaller than  $D$  meters (m). In parallel, let  $z_\ell \in \{0, 1\}$  indicate whether an IRS is installed at candidate site  $\ell$ , where  $z_\ell = 1$  means selected and 0 otherwise. While  $z_\ell$  is area-independent, the IRS phase shifts are area-adaptive. For a deployed IRS at site  $\ell$ , the diagonal phase-shift matrix for area  $j$  is given by  $\Theta_{\ell,j} = \text{diag}(e^{j\psi_{\ell,1,j}}, \dots, e^{j\psi_{\ell,N_\ell,j}}) \in \mathbb{C}^{N_\ell \times N_\ell}$ ,

with  $\psi_{\ell,n,j} \in [0, 2\pi)$  denoting the phase shift of element  $n \in \mathcal{N}_\ell \triangleq \{1, \dots, N_\ell\}$ .

The MA moving region and the physical size of each IRS are assumed to be much smaller than the corresponding link distances. Hence, all propagation paths can be treated as operating in the far field. Under this condition, relocating an MA influences only the phase of the associated channel coefficient, whereas the angle of departure (AoD), angle of arrival (AoA), and amplitude can be regarded as invariant [20]. Furthermore, IRS-related links are treated as LoS-dominant under the assumption that the candidate sites are deliberately selected at elevated, unobstructed locations. If an IRS is placed at candidate location  $\ell \in \mathcal{L}$  (i.e.,  $z_\ell = 1$ ), the BS-to-IRS channel when serving target area  $j$  can be modeled as

$$\begin{aligned} \mathbf{G}_\ell(\mathbf{x}_j) &= \sqrt{C_0 d_\ell^{-2}} \\ &\times \left[ 1, e^{j\frac{2\pi}{\lambda}(\mathbf{p}_{\ell,2} - \mathbf{p}_{\ell,1})^T \mathbf{a}(\theta_{\ell,1}^r, \phi_{\ell,1}^r)}, \dots, e^{j\frac{2\pi}{\lambda}(\mathbf{p}_{\ell,N_\ell} - \mathbf{p}_{\ell,1})^T \mathbf{a}(\theta_{\ell,1}^r, \phi_{\ell,1}^r)} \right]^H \\ &\times \left( \mathbf{x}_j^T \odot \left[ e^{j\frac{2\pi}{\lambda} \mathbf{t}_1^T \mathbf{a}(\theta_{\ell,1}^t, \phi_{\ell,1}^t)}, \dots, e^{j\frac{2\pi}{\lambda} \mathbf{t}_{N_\ell}^T \mathbf{a}(\theta_{\ell,1}^t, \phi_{\ell,1}^t)} \right] \right) \in \mathbb{C}^{N_\ell \times M}, \end{aligned} \quad (2)$$

with  $\mathbf{x}_j \triangleq [x_{1,j}, \dots, x_{M,j}]^T \in \{0, 1\}^M$  representing the MA configuration for area  $j$ , and  $d_\ell \triangleq \|\mathbf{p}_{\ell,1}\|$  the distance from the BS reference point to the IRS reference point. The scalar  $C_0 d_\ell^{-2}$  accounts for the large-scale path loss, with  $C_0$  denoting the path-loss coefficient at the reference distance of 1 m. In addition,  $\mathbf{a}(\theta_{\ell,1}^t, \phi_{\ell,1}^t) \triangleq [\cos \theta_{\ell,1}^t \cos \phi_{\ell,1}^t, \cos \theta_{\ell,1}^t \sin \phi_{\ell,1}^t, \sin \theta_{\ell,1}^t]^T$  and  $\mathbf{a}(\theta_{\ell,1}^r, \phi_{\ell,1}^r) \triangleq [\cos \theta_{\ell,1}^r \cos \phi_{\ell,1}^r, \cos \theta_{\ell,1}^r \sin \phi_{\ell,1}^r, \sin \theta_{\ell,1}^r]^T$  represent the normalized transmit and receive direction vectors, respectively [23]. The parameters  $\theta_{\ell,1}^t$  and  $\phi_{\ell,1}^t$  are the elevation AoD and azimuth AoD at the BS, while  $\theta_{\ell,1}^r$  and  $\phi_{\ell,1}^r$  are the elevation AoA and azimuth AoA at the IRS. To express  $\mathbf{G}_\ell(\mathbf{x}_j)$  in a more compact form, we further define  $\mathbf{e}_\ell \triangleq \left[ 1, e^{j\frac{2\pi}{\lambda}(\mathbf{p}_{\ell,2} - \mathbf{p}_{\ell,1})^T \mathbf{a}(\theta_{\ell,1}^r, \phi_{\ell,1}^r)}, \dots, e^{j\frac{2\pi}{\lambda}(\mathbf{p}_{\ell,N_\ell} - \mathbf{p}_{\ell,1})^T \mathbf{a}(\theta_{\ell,1}^r, \phi_{\ell,1}^r)} \right]^H \in \mathbb{C}^{N_\ell \times 1}$ ,  $\mathbf{g}_\ell^H \triangleq \left[ e^{j\frac{2\pi}{\lambda} \mathbf{t}_1^T \mathbf{a}(\theta_{\ell,1}^t, \phi_{\ell,1}^t)}, \dots, e^{j\frac{2\pi}{\lambda} \mathbf{t}_{N_\ell}^T \mathbf{a}(\theta_{\ell,1}^t, \phi_{\ell,1}^t)} \right]^H \in \mathbb{C}^{1 \times M}$ ,  $\mathbf{X}_j \triangleq \text{diag}(\mathbf{x}_j)$ , and  $\overline{\mathbf{G}}_\ell \triangleq \sqrt{C_0 d_\ell^{-2}} \mathbf{e}_\ell \mathbf{g}_\ell^H$ . Then,  $\mathbf{G}_\ell(\mathbf{x}_j)$  can be rewritten as

$$\begin{aligned} \mathbf{G}_\ell(\mathbf{x}_j) &= \sqrt{C_0 d_\ell^{-2}} \mathbf{e}_\ell (\mathbf{x}_j^T \odot \mathbf{g}_\ell^H) = \sqrt{C_0 d_\ell^{-2}} \mathbf{e}_\ell \mathbf{g}_\ell^H \mathbf{X}_j \\ &= \overline{\mathbf{G}}_\ell \mathbf{X}_j. \end{aligned} \quad (3)$$

Similarly, the channel from the IRS at candidate site  $\ell$  to location  $\mathbf{u}_j$  is modeled as

$$\begin{aligned} \mathbf{h}_\ell^H(\mathbf{u}_j) &= \sqrt{C_0 \tilde{d}_\ell(\mathbf{u}_j)^{-2}} \\ &\times \left[ 1, e^{j\frac{2\pi}{\lambda}(\mathbf{p}_{\ell,2} - \mathbf{p}_{\ell,1})^T \mathbf{a}(\theta_{\ell,j}^t, \phi_{\ell,j}^t(\mathbf{u}_j))}, \dots, \right. \\ &\left. e^{j\frac{2\pi}{\lambda}(\mathbf{p}_{\ell,N_\ell} - \mathbf{p}_{\ell,1})^T \mathbf{a}(\theta_{\ell,j}^t, \phi_{\ell,j}^t(\mathbf{u}_j))} \right] \in \mathbb{C}^{1 \times N_\ell}, \end{aligned} \quad (4)$$

where  $\tilde{d}_\ell(\mathbf{u}_j) \triangleq \|\mathbf{p}_{\ell,1} - \mathbf{u}_j\|$  denotes the distance between the IRS reference point and  $\mathbf{u}_j$ , and  $\mathbf{a}(\theta_{\ell,j}^t(\mathbf{u}_j), \phi_{\ell,j}^t(\mathbf{u}_j)) \triangleq [\cos \theta_{\ell,j}^t(\mathbf{u}_j) \cos \phi_{\ell,j}^t(\mathbf{u}_j), \cos \theta_{\ell,j}^t(\mathbf{u}_j) \sin \phi_{\ell,j}^t(\mathbf{u}_j), \sin \theta_{\ell,j}^t(\mathbf{u}_j)]^T$  denotes the normalized wave vector, with  $\theta_{\ell,j}^t(\mathbf{u}_j)$  and  $\phi_{\ell,j}^t(\mathbf{u}_j)$  being the elevation and azimuth AoDs towards  $\mathbf{u}_j$ , respectively.

Let  $P$  denote the transmit power and define an  $M$ -dimensional beamforming vector  $\mathbf{w}_{\mathbf{u}_j} \in \mathbb{C}^{M \times 1}$  associated with all candidate MA positions for location  $\mathbf{u}_j$ . The effective beamforming vector is then given by

$$\tilde{\mathbf{w}}_{\mathbf{u}_j} = \mathbf{X}_j \mathbf{w}_{\mathbf{u}_j} \in \mathbb{C}^{M \times 1}, \quad (5)$$

where  $\tilde{\mathbf{w}}_{\mathbf{u}_j}$  retains the beamforming coefficients at candidate positions occupied by MAs and forces the coefficients at all other positions to zero. Neglecting the signal components resulting from double or multiple reflections at the deployed IRSs, the received SNR at location  $\mathbf{u}_j \in \mathcal{A}_j$ ,  $j \in \mathcal{J}$  can be written as

$$\begin{aligned} \gamma_{\mathbf{u}_j} &= \bar{P} \left| \left( \sum_{\ell=1}^L z_{\ell} \mathbf{h}_{\ell}^H(\mathbf{u}_j) \Theta_{\ell,j} \bar{\mathbf{G}}_{\ell} \mathbf{X}_j \right) \mathbf{X}_j \mathbf{w}_{\mathbf{u}_j} \right|^2 \\ &= \bar{P} \left| \left( \sum_{\ell=1}^L z_{\ell} \mathbf{h}_{\ell}^H(\mathbf{u}_j) \Theta_{\ell,j} \bar{\mathbf{G}}_{\ell} \right) \mathbf{X}_j \mathbf{w}_{\mathbf{u}_j} \right|^2, \end{aligned} \quad (6)$$

where  $\bar{P} \triangleq \frac{P}{\sigma^2}$  with  $\sigma^2$  representing the noise power at location  $\mathbf{u}$ , and the second equality follows from the idempotence of the binary diagonal matrix  $\mathbf{X}_j$ , i.e.,  $\mathbf{X}_j^2 = \mathbf{X}_j$ .

Let  $c_{\text{MA}}$  denote the unit cost per MA. Since the  $J$  target areas are served sequentially and the same hardware can be reused across areas, the required number of MAs is determined by the maximum number of active MAs over all areas, i.e.,  $\max_{j \in \mathcal{J}} \left\{ \sum_{m=1}^M x_{m,j} \right\}$ . The corresponding MA deployment cost is therefore modeled as  $c_{\text{MA}} \max_{j \in \mathcal{J}} \left\{ \sum_{m=1}^M x_{m,j} \right\}$ . Similarly, the IRS deployment cost is given by  $\sum_{\ell=1}^L z_{\ell} (c_{\ell} + c_{\text{e}} N_{\ell})$ , where  $c_{\ell}$  is the site-specific installation cost at candidate site  $\ell$  (reflecting, e.g., terrain, leasing and installation complexity), and  $c_{\text{e}}$  denotes the unit cost per IRS element. Combining both contributions, the total infrastructure deployment cost is

$$C_{\text{tot}} = c_{\text{MA}} \max_{j \in \mathcal{J}} \left\{ \sum_{m=1}^M x_{m,j} \right\} + \sum_{\ell=1}^L z_{\ell} (c_{\ell} + c_{\text{e}} N_{\ell}). \quad (7)$$

### B. Problem Formulation

In this paper, we aim to minimize the total deployment cost by jointly selecting the IRS sites, determining the MA placements and hence the number of deployed MAs, optimizing the IRS phase shifts and the BS transmit beamforming vectors, while guaranteeing SNR requirements for all target areas. The problem of interest can be formulated as

$$\begin{aligned} (\text{P1}) : \quad & \min_{\{x_{m,j}\}, \{z_{\ell}\}, \{\Theta_{\ell,j}\}, \{\mathbf{w}_{\mathbf{u}_j}\}} \quad c_{\text{MA}} \max_{j \in \mathcal{J}} \left\{ \sum_{m=1}^M x_{m,j} \right\} \\ & + \sum_{\ell=1}^L z_{\ell} (c_{\ell} + c_{\text{e}} N_{\ell}) \end{aligned} \quad (8a)$$

$$\text{s.t.} \quad \bar{P} \left| \left( \sum_{\ell=1}^L z_{\ell} \mathbf{h}_{\ell}^H(\mathbf{u}_j) \Theta_{\ell,j} \bar{\mathbf{G}}_{\ell} \right) \mathbf{X}_j \mathbf{w}_{\mathbf{u}_j} \right|^2 \geq \gamma_{\text{th},j}, \quad (8b)$$

$$\forall \mathbf{u}_j \in \mathcal{A}_j, j \in \mathcal{J}, \quad (8c)$$

$$\mathbf{X}_j = \text{diag} (x_{1,j}, x_{2,j}, \dots, x_{M,j}), \quad \forall j \in \mathcal{J}, \quad (8d)$$

$$x_{m,j} \in \{0, 1\}, \quad \forall m \in \mathcal{M}, j \in \mathcal{J}, \quad (8e)$$

$$x_{m,j} + x_{q,j} \leq 1, \quad \forall (m, q) \in \mathcal{D}, j \in \mathcal{J}, \quad (8f)$$

$$\sum_{m=1}^M x_{m,j} \leq M_{\text{max}}, \quad \forall j \in \mathcal{J}, \quad (8g)$$

$$z_{\ell} \in \{0, 1\}, \quad \forall \ell \in \mathcal{L}, \quad (8h)$$

$$\sum_{\ell=1}^L z_{\ell} \leq L, \quad (8i)$$

$$\left| [\Theta_{\ell,j}]_{n,n} \right| = 1, \quad \forall \ell \in \mathcal{L}, j \in \mathcal{J}, n \in \mathcal{N}_{\ell}, \quad (8j)$$

where (8b) ensures that the received SNR at any location  $\mathbf{u}_j$  in area  $j$  is no less than a predefined threshold  $\gamma_{\text{th},j}$ , and (8c) ensures that the effective beamforming vector for  $\mathbf{u}_j$  has an unit norm. For the MA configuration, (8d) and (8e) define the binary placement decisions. The selected MA positions are subject to the minimum-separation requirement captured by the conflict set  $\mathcal{D}$  in (8f), which, together with the moving region and the grid step size  $d$ , specifies the upper bound  $M_{\text{max}}$  on the number of simultaneously deployable MAs in (8g). Finally, (8h)-(8j) limit the total number of deployable IRSs and imposes the modulus constraint on the IRS reflection coefficients.

Problem (P1) is challenging to solve due to: 1) the hybrid discrete-continuous variables; 2) the semi-infinite SNR constraints arising from continuous target areas; and 3) the inherent non-convexity of the SNR and unit-modulus constraints. Hence, (P1) is a mixed-integer non-convex program, and computing a globally optimal solution is generally prohibitive.

### III. FEASIBILITY CHECK

Before solving problem (P1), we first check its feasibility. Specifically, note that if the SNR targets in (P1) cannot be satisfied even under the most favorable deployment configuration, then problem (P1) is infeasible regardless of the cost coefficients. To this end, we consider an auxiliary feasibility check problem where all candidate IRSs are activated and the BS is permitted to deploy at most  $M_{\text{max}}$  MAs for each target area. Concretely, we set  $z_{\ell} = 1, \forall \ell \in \mathcal{L}$ , and introduce a non-negative slack variable  $\eta$  as the common lower bound of the normalized SNR, namely, the received SNR divided by the corresponding threshold. The feasibility check problem is formulated as

$$(\text{P2}) : \quad \max_{\{x_{m,j}\}, \{\Theta_{\ell,j}\}, \{\mathbf{w}_{\mathbf{u}_j}\}, \{\eta\}, \eta \geq 0} \eta \quad (9a)$$

$$\text{s.t.} \quad \frac{\bar{P}}{\gamma_{\text{th},j}} \left| \left( \sum_{\ell=1}^L \mathbf{h}_{\ell}^H(\mathbf{u}_j) \Theta_{\ell,j} \bar{\mathbf{G}}_{\ell} \right) \mathbf{X}_j \mathbf{w}_{\mathbf{u}_j} \right|^2 \geq \eta, \quad (9b)$$

$$\forall \mathbf{u}_j \in \mathcal{A}_j, \quad \forall j \in \mathcal{J}, \quad (9c)$$

$$(8c) - (8g), (8j). \quad (9c)$$

Note that the MA placement achieving the maximum cardinality  $M_{\text{max}}$  is not necessarily unique. Moreover, a fully populated array can be forced into geometrically suboptimal locations, and the SNR-optimal MA configuration may differ across target areas. Thus, even with  $M_{\text{max}}$  fixed, the placement

variables  $\{x_{m,j}\}$  must still be optimized. Let  $\eta^*$  be the optimal value of problem (P2). If  $\eta^* \geq 1$ , the SNR requirements in problem (P1) are achievable, and we proceed to solve (P1) for cost minimization; otherwise, (P1) is infeasible.

Next, we solve the feasibility check problem (P2). It can be readily verified that the optimal transmit beamformer  $\mathbf{w}_{\mathbf{u}_j}^*$  follows the maximum-ratio-transmission (MRT) principle:

$$\mathbf{w}_{\mathbf{u}_j}^* = \frac{\mathbf{X}_j \left( \sum_{\ell=1}^L \mathbf{h}_\ell^H(\mathbf{u}_j) \Theta_{\ell,j} \bar{\mathbf{G}}_\ell \right)^H}{\left\| \mathbf{X}_j \left( \sum_{\ell=1}^L \mathbf{h}_\ell^H(\mathbf{u}_j) \Theta_{\ell,j} \bar{\mathbf{G}}_\ell \right)^H \right\|^2}. \quad (10)$$

Substituting (10) into problem (P2) yields

$$\max_{\{x_{m,j}\}, \{\Theta_{\ell,j}\}, \eta \geq 0} \eta \quad (11a)$$

$$\text{s.t. } \frac{\bar{P}}{\gamma_{\text{th},j}} \left\| \left( \sum_{\ell=1}^L \mathbf{h}_\ell^H(\mathbf{u}_j) \Theta_{\ell,j} \bar{\mathbf{G}}_\ell \right) \mathbf{X}_j \right\|^2 \geq \eta, \quad (11b)$$

$$\forall \mathbf{u}_j \in \mathcal{A}_j, \forall j \in \mathcal{J}, \quad (11b)$$

$$(8d) - (8g), (8j). \quad (11c)$$

Problem (11) poses significant challenges due to the semi-infinite SNR constraints induced by the continuous target areas  $\{\mathcal{A}_j\}$ , the coupling of optimization variables in (11b), and the non-convex constraints (8e) and (8j). To make the problem tractable, we first approximate the semi-infinite constraints by discretizing each  $\mathcal{A}_j$  into a dense grid  $\mathcal{G}_j$  and enforcing (11b) only over  $\mathcal{G}_j$ , yielding

$$\max_{\{x_{m,j}\}, \{\Theta_{\ell,j}\}, \eta \geq 0} \eta \quad (12a)$$

$$\text{s.t. } \frac{\bar{P}}{\gamma_{\text{th},j}} \left\| \left( \sum_{\ell=1}^L \mathbf{h}_\ell^H(\mathbf{u}_j) \Theta_{\ell,j} \bar{\mathbf{G}}_\ell \right) \mathbf{X}_j \right\|^2 \geq \eta, \quad (12b)$$

$$\forall \mathbf{u}_j \in \mathcal{G}_j, \forall j \in \mathcal{J}, \quad (12b)$$

$$(8d) - (8g), (8j). \quad (12c)$$

Problem (12) serves as a discretized approximation of problem (11). For static LoS channels, a high-resolution offline grid can keep the approximation error small. Although discretization removes infinitely many constraints, the variable coupling and non-convexity persist. To address these remaining issues, we employ an AO framework that alternately optimizes  $\{x_{m,j}\}$  and  $\{\Theta_{\ell,j}\}$  until convergence, as detailed below.

#### A. Optimizing $\{x_{m,j}\}$ for Given $\{\Theta_{\ell,j}\}$

When  $\{\Theta_{\ell,j}\}$  is fixed, problem (12) reduces to

$$\max_{\{x_{m,j}\}, \eta \geq 0} \eta \quad \text{s.t. (12b), (8d) - (8g).} \quad (13)$$

To facilitate the solution design, we expand the quadratic term  $\left\| \left( \sum_{\ell=1}^L \mathbf{h}_\ell^H(\mathbf{u}_j) \Theta_{\ell,j} \bar{\mathbf{G}}_\ell \right) \mathbf{X}_j \right\|^2$  in constraint (12b) as

$$\begin{aligned} & \left\| \left( \sum_{\ell=1}^L \mathbf{h}_\ell^H(\mathbf{u}_j) \Theta_{\ell,j} \bar{\mathbf{G}}_\ell \right) \mathbf{X}_j \right\|^2 \\ &= \sum_{m=1}^M x_{m,j} \left| \sum_{\ell=1}^L \mathbf{h}_\ell^H(\mathbf{u}_j) \Theta_{\ell,j} \bar{\mathbf{G}}_\ell(:, m) \right|^2 \end{aligned}$$

$$\triangleq \sum_{m=1}^M x_{m,j} C_{m,j}(\mathbf{u}_j), \quad (14)$$

where  $C_{m,j}(\mathbf{u}_j) \triangleq \left| \sum_{\ell=1}^L \mathbf{h}_\ell^H(\mathbf{u}_j) \Theta_{\ell,j} \bar{\mathbf{G}}_\ell(:, m) \right|^2$ . Substituting (14) into problem (13) yields the following equivalent formulation:

$$\max_{\{x_{m,j}\}, \eta \geq 0} \eta \quad (15a)$$

$$\text{s.t. } \frac{\bar{P}}{\gamma_{\text{th},j}} \sum_{m=1}^M x_{m,j} C_{m,j}(\mathbf{u}_j) \geq \eta, \forall \mathbf{u}_j \in \mathcal{G}_j, \forall j \in \mathcal{J}, \quad (15b)$$

$$(8e) - (8g), \quad (15c)$$

Problem (15) is a mixed-integer linear program (MILP). Although it can be solved by off-the-shelf MILP solvers (e.g., MOSEK), calling an exact integer solver at each AO iteration becomes computationally prohibitive in large-scale settings due to the exponential worst-case complexity of integer programming. To obtain a scalable, polynomial-time update that can be embedded into the iterative framework, we adopt a penalty-based continuous reformulation of the binary constraint (8e). Specifically, (8e) is equivalent to the intersection of the following two inequalities:

$$0 \leq x_{m,j} \leq 1, \forall m \in \mathcal{M}, j \in \mathcal{J}, \quad (16a)$$

$$x_{m,j} - x_{m,j}^2 \leq 0, \forall m \in \mathcal{M}, j \in \mathcal{J}. \quad (16b)$$

Here, (16a) defines a convex set, whereas (16b) is a non-convex constraint in the difference-of-convex form. To tackle the non-convexity in (16b), we adopt the SCA technique by linearizing the quadratic term  $x_{m,j}^2$  via the first-order Taylor expansion at a given local point  $x_{m,j}^r$  in the  $r$ -th iteration. This yields the following global affine lower bound:

$$\begin{aligned} x_{m,j}^2 &\geq - (x_{m,j}^r)^2 + 2x_{m,j}^r x_{m,j} \\ &\triangleq \Pi^{\text{lb},r}(x_{m,j}), \forall m \in \mathcal{M}, j \in \mathcal{J}. \end{aligned} \quad (17)$$

Substituting this lower bound into (16b) yields the convex surrogate constraint  $x_{m,j} - \Pi^{\text{lb},r}(x_{m,j}) \leq 0, \forall m \in \mathcal{M}, j \in \mathcal{J}$ . However, imposing this SCA-based surrogate as a hard constraint together with the box constraint (16a) may result in overly conservative updates, which can significantly shrink the feasible region and even lead to algorithm stagnation in practice. To maintain sufficient update flexibility while still promoting integrality, we instead penalize the violation of the surrogate constraint in the objective of problem (15). This gives the following penalized formulation:

$$\max_{\{x_{m,j}\}, \eta \geq 0} \eta - \rho \sum_{m=1}^M \sum_{j=1}^J (x_{m,j} - \Pi^{\text{lb},r}(x_{m,j})) \quad (18a)$$

$$\text{s.t. (16a), (15b), (8f) - (8g),} \quad (18b)$$

where  $\rho > 0$  is a penalty factor used to control the tightness of the relaxation. Problem (18) is a convex linear program, which can be efficiently solved using standard tools such as CVX. As the SCA iterations proceed, the linearization becomes tight, and  $x_{m,j} - \Pi^{\text{lb},r}(x_{m,j})$  approaches  $x_{m,j} - x_{m,j}^2 = x_{m,j}(1 - x_{m,j})$ . Since this term is subtracted in the maximization objective, a sufficiently large  $\rho$  strongly discourages fractional

$x_{m,j} \in (0, 1)$  and drives  $x_{m,j} - \Pi^{\text{lb},r}(x_{m,j})$  towards zero. Together with the box constraint  $0 \leq x_{m,j} \leq 1$ , this promotes  $x_{m,j}(1 - x_{m,j}) \rightarrow 0$ , thereby pushing  $x_{m,j}$  towards  $\{0, 1\}$ .

### B. Optimizing $\{\Theta_{\ell,j}\}$ for Given $\{x_{m,j}\}$

With  $\{x_{m,j}\}$  fixed, the optimization of  $\{\Theta_{\ell,j}\}$  reduces to solving problem (12) subject to constraints (12b) and (8j). To streamline the formulation and expose the curvature of the key term, we define the aggregate dimension  $N \triangleq \sum_{\ell=1}^L N_{\ell}$ , the stacked channel vector  $\mathbf{h}^H(\mathbf{u}_j) \triangleq [\mathbf{h}_1^H(\mathbf{u}_j), \dots, \mathbf{h}_L^H(\mathbf{u}_j)] \in \mathbb{C}^{1 \times N}$ , the stacked channel matrix  $\bar{\mathbf{G}} \triangleq [\bar{\mathbf{G}}_1^T, \dots, \bar{\mathbf{G}}_L^T]^T \in \mathbb{C}^{N \times M}$ , and the cascaded channel matrix  $\Psi(\mathbf{u}_j) \triangleq \text{diag}(\mathbf{h}^H(\mathbf{u}_j)) \bar{\mathbf{G}} \in \mathbb{C}^{N \times M}$ . Further, let  $\Theta_j \triangleq \text{blkdiag}(\Theta_{1,j}, \dots, \Theta_{L,j}) \in \mathbb{C}^{N \times N}$  and  $\mathbf{v}_j \triangleq \text{diag}(\Theta_j^H) \in \mathbb{C}^{N \times 1}$ . Then, the quadratic term in (12b) can be recast as

$$\begin{aligned} \left\| \left( \sum_{\ell=1}^L \mathbf{h}_{\ell}^H(\mathbf{u}_j) \Theta_{\ell,j} \bar{\mathbf{G}}_{\ell} \right) \mathbf{X}_j \right\|^2 &= \|\mathbf{h}^H(\mathbf{u}_j) \Theta_j \bar{\mathbf{G}} \mathbf{X}_j\|^2 \\ &= \|\mathbf{v}_j^H \Psi(\mathbf{u}_j) \mathbf{X}_j\|^2 \triangleq \mathbf{v}_j^H \mathbf{R}(\mathbf{u}_j) \mathbf{v}_j, \end{aligned} \quad (19)$$

where  $\mathbf{R}(\mathbf{u}_j) \triangleq \Psi(\mathbf{u}_j) \mathbf{X}_j \mathbf{X}_j^H \Psi^H(\mathbf{u}_j)$ . Consequently, the subproblem is equivalent to

$$\max_{\{\mathbf{v}_j\}, \eta} \eta \quad (20a)$$

$$\text{s.t. } \frac{\bar{P}}{\gamma_{\text{th},j}} \mathbf{v}_j^H \mathbf{R}(\mathbf{u}_j) \mathbf{v}_j \geq \eta, \quad \forall \mathbf{u}_j \in \mathcal{G}_j, \forall j \in \mathcal{J}, \quad (20b)$$

$$|\mathbf{v}_j|_n = 1, \quad \forall j \in \mathcal{J}, \quad n \in \mathcal{N}, \quad (20c)$$

where  $\mathcal{N}$  denotes the set of all IRS elements. Since  $\mathbf{R}(\mathbf{u}_j) \succeq 0$ , the term  $\mathbf{v}_j^H \mathbf{R}(\mathbf{u}_j) \mathbf{v}_j$  is convex, rendering constraint (20b) non-convex. To address this, we adopt the SCA framework and linearize  $\mathbf{v}_j^H \mathbf{R}(\mathbf{u}_j) \mathbf{v}_j$  at a given local point  $\mathbf{v}_j^r$  to obtain the following affine lower bound:

$$\begin{aligned} \mathbf{v}_j^H \mathbf{R}(\mathbf{u}_j) \mathbf{v}_j &\geq 2\Re\left\{(\mathbf{v}_j^r)^H \mathbf{R}(\mathbf{u}_j) \mathbf{v}_j\right\} - (\mathbf{v}_j^r)^H \mathbf{R}(\mathbf{u}_j) \mathbf{v}_j^r \\ &\triangleq \Xi^{\text{lb},r}(\mathbf{v}_j, \mathbf{u}_j). \end{aligned} \quad (21)$$

Accordingly, the non-convex constraint (20b) is approximated by the following convex constraint:

$$\frac{\bar{P}}{\gamma_{\text{th},j}} \Xi^{\text{lb},r}(\mathbf{v}_j, \mathbf{u}_j) \geq \eta, \quad \forall \mathbf{u}_j \in \mathcal{G}_j, \forall j \in \mathcal{J}. \quad (22)$$

Next, we handle the unit-modulus constraints in (20c), which can be written as the following pair of inequalities:

$$1 \leq |\mathbf{v}_j|_n^2, \quad \forall j \in \mathcal{J}, \quad n \in \mathcal{N}, \quad (23a)$$

$$|\mathbf{v}_j|_n^2 \leq 1, \quad \forall j \in \mathcal{J}, \quad n \in \mathcal{N}. \quad (23b)$$

It is clear that (23b) is convex, whereas (23a) is non-convex. To obtain a tractable inner approximation of (23a), we linearize  $|\mathbf{v}_j|_n^2$  at the local point  $|\mathbf{v}_j^r|_n$  as

$$\begin{aligned} |\mathbf{v}_j|_n^2 &\geq 2\Re\left\{(\mathbf{v}_j^r)_n^* |\mathbf{v}_j|_n\right\} - |\mathbf{v}_j^r|_n^2 \\ &\triangleq \chi^{\text{lb},r}(|\mathbf{v}_j|_n). \end{aligned} \quad (24)$$

Replacing  $|\mathbf{v}_j|_n^2$  in (23a) by  $\chi^{\text{lb},r}(|\mathbf{v}_j|_n)$  yields the SCA surrogate constraint  $1 \leq \chi^{\text{lb},r}(|\mathbf{v}_j|_n), \forall j \in \mathcal{J}, n \in \mathcal{N}$ . Similar to the previous subsection, enforcing this surrogate constraint along with the unit-disc constraint (23b) may be overly restrictive and hinder iterative progress. To alleviate this issue, we adopt the penalty method. However, unlike the binary case in (18), directly penalizing  $1 - \chi^{\text{lb},r}(|\mathbf{v}_j|_n)$  in the objective function is generally undesirable. Minimizing  $1 - \chi^{\text{lb},r}(|\mathbf{v}_j|_n)$  is equivalent to maximizing the affine lower bound  $\chi^{\text{lb},r}(|\mathbf{v}_j|_n)$ , which, under the unit-disc constraint (23b), reduces to maximizing  $\Re\left\{(\mathbf{v}_j^r)_n^* |\mathbf{v}_j|_n\right\}$ . This tends to phase-align  $|\mathbf{v}_j|_n$  with  $|\mathbf{v}_j^r|_n$ , leading to overly conservative updates. Such conservatism may cause premature stagnation and impede the improvement of  $\eta$  over iterations.

Instead, we introduce non-negative slack variables  $\{\delta_{j,n}\}$  to relax the SCA surrogate constraint as

$$1 - \delta_{j,n} \leq \chi^{\text{lb},r}(|\mathbf{v}_j|_n), \quad \forall j \in \mathcal{J}, \quad n \in \mathcal{N}, \quad (25)$$

where  $\delta_{j,n} \geq 0$  quantifies the violation of (23a) in the current iteration. We then penalize  $\{\delta_{j,n}\}$  in the objective. This yields a one-sided (hinge-loss) penalty: the penalty is activated only when  $1 > \chi^{\text{lb},r}(|\mathbf{v}_j|_n)$ , whereas  $\delta_{j,n} = 0$  once the surrogate constraint is satisfied, thereby avoiding an unnecessary incentive to further increase  $\chi^{\text{lb},r}(|\mathbf{v}_j|_n)$ . Accordingly, the phase-update subproblem in the  $r$ -th SCA iteration is formulated as

$$\max_{\{\mathbf{v}_j\}, \eta} \eta - \lambda \sum_{j \in \mathcal{J}} \sum_{n \in \mathcal{N}} \delta_{j,n} \quad (26a)$$

$$\text{s.t. } (22), (23b), (25), \quad (26b)$$

where  $\lambda > 0$  is a penalty factor. At optimality, the slack variable satisfies  $\delta_{j,n} = [1 - \chi^{\text{lb},r}(|\mathbf{v}_j|_n)]_+$ . With a properly chosen (or gradually increased)  $\lambda$ , the slack variables  $\{\delta_{j,n}\}$  tend to vanish, thereby promoting  $|\mathbf{v}_j|_n \rightarrow 1$ . Problem (26) is a convex quadratically constrained quadratic program (QCQP) and can be efficiently solved using standard tools, e.g., CVX.

### C. Overall Algorithm

The proposed algorithm adopts a **double-loop structure** to solve the original non-convex problem (12). In the **inner loop**, the penalty factors  $\rho$  and  $\lambda$  are held fixed. Utilizing the AO framework, the variables  $\{x_{m,j}\}$  and  $\{\Theta_{\ell,j}\}$  are alternately optimized by solving subproblems (18) and (26). Based on the standard complexity result of interior-point methods [40], the computational complexity of solving (18) is  $\mathcal{O}\left((G + 2MJ)^{1.5} (MJ)^2 \ln(1/\epsilon)\right)$ , while solving (26) requires a computational complexity of  $\mathcal{O}\left((JN)^2 (JN + G)^{1.5} \ln(1/\epsilon)\right)$ , where  $G \triangleq \sum_{j=1}^J |\mathcal{G}_j|$  and  $\epsilon$  denotes the solution accuracy. The AO continues until the joint penalized objective,  $\eta - \rho \sum_{m=1}^M \sum_{j=1}^J (x_{m,j} - \Pi^{\text{lb},r}(x_{m,j})) - \lambda \sum_{j \in \mathcal{J}} \sum_{n \in \mathcal{N}} \delta_{j,n}$ , converges for a given pair of  $\{\rho, \lambda\}$ . In the **outer loop**, we evaluate the constraint violations. If the binary or unit-modulus constraints are not satisfied, the penalty factors  $\rho$  and  $\lambda$  are increased (for instance, by multiplying by a scaling

factor  $\mu > 1$ ), and the inner loop is restarted. This procedure continues until the maximum constraint violation falls below a predefined tolerance.

Finally, we briefly discuss the convergence of the proposed algorithm. With fixed penalty factors, the AO inner loop generates a non-decreasing objective sequence, which is upper-bounded over the feasible set. Hence, the inner loop converges to a stationary point. In the outer loop, the penalty factors  $\rho$  and  $\lambda$  are progressively increased, driving the penalized constraint violations to vanish as  $\rho, \lambda \rightarrow \infty$ . Consequently, the final solution satisfies the original binary and unit-modulus constraints and provides a feasible starting point for solving the cost minimization problem (P1) in the next section.

#### IV. PROPOSED ALGORITHM FOR PROBLEM (P1)

In this section, we solve problem (P1). First, analogous to (10), the optimal transmit beamformer  $\mathbf{w}_{\mathbf{u}_j}^*$  is given by

$$\mathbf{w}_{\mathbf{u}_j}^* = \frac{\mathbf{X}_j \left( \sum_{\ell=1}^L z_{\ell} \mathbf{h}_{\ell}^H(\mathbf{u}_j) \Theta_{\ell,j} \bar{\mathbf{G}}_{\ell} \right)^H}{\left\| \mathbf{X}_j \left( \sum_{\ell=1}^L z_{\ell} \mathbf{h}_{\ell}^H(\mathbf{u}_j) \Theta_{\ell,j} \bar{\mathbf{G}}_{\ell} \right)^H \right\|}. \quad (27)$$

By substituting (27) into (P1) and adopting the grid-based discretization strategy to handle the semi-infinite SNR constraints (replacing  $\mathcal{A}_j$  with  $\mathcal{G}_j$  as in (12)), we arrive at the following reformulated problem:

$$\min_{\{x_{m,j}\}, \{z_{\ell}\}, \{\Theta_{\ell,j}\}} c_{\text{MA}} \max_{j \in \mathcal{J}} \left\{ \sum_{m=1}^M x_{m,j} \right\} + \sum_{\ell=1}^L z_{\ell} (c_{\ell} + c_{\text{e}} N_{\ell}) \quad (28a)$$

$$\text{s.t. } \bar{P} \left\| \left( \sum_{\ell=1}^L z_{\ell} \mathbf{h}_{\ell}^H(\mathbf{u}_j) \Theta_{\ell,j} \bar{\mathbf{G}}_{\ell} \right) \mathbf{X}_j \right\|^2 \geq \gamma_{\text{th},j}, \quad (28b)$$

$$\forall \mathbf{u}_j \in \mathcal{G}_j, j \in \mathcal{J}, \quad (28c)$$

$$(8d) - (8j). \quad (28d)$$

Despite improved tractability, problem (28) remains non-convex due to the coupled variables and the binary/unit-modulus constraints. We tackle these challenges using a double-loop framework similar to that in Section III, initialized with the feasible solution obtained therein. Specifically, the inner loop alternately updates the two variable blocks  $\{x_{m,j}, z_{\ell}\}$  and  $\{\Theta_{\ell,j}\}$  with fixed penalty factors, while the outer loop progressively increases penalties to drive constraint violations to zero. The two subproblems are derived below.

##### A. Optimizing $\{x_{m,j}, z_{\ell}\}$ for Given $\{\Theta_{\ell,j}\}$

With given  $\{\Theta_{\ell,j}\}$ , the binary indicators  $\{x_{m,j}, z_{\ell}\}$  can be jointly optimized by solving the following subproblem of (28):

$$\min_{\{x_{m,j}\}, \{z_{\ell}\}} c_{\text{MA}} \max_{j \in \mathcal{J}} \left\{ \sum_{m=1}^M x_{m,j} \right\} + \sum_{\ell=1}^L z_{\ell} (c_{\ell} + c_{\text{e}} N_{\ell}) \quad (29a)$$

$$\text{s.t. } (28b), (8d) - (8i). \quad (29b)$$

To make the coupling structure in constraint (28b) more explicit, we expand the term  $\left\| \left( \sum_{\ell=1}^L z_{\ell} \mathbf{h}_{\ell}^H(\mathbf{u}_j) \Theta_{\ell,j} \bar{\mathbf{G}}_{\ell} \right) \mathbf{X}_j \right\|^2$

and express it explicitly in terms of  $\{x_{m,j}, z_{\ell}\}$  as follows:

$$\begin{aligned} & \left\| \left( \sum_{\ell=1}^L z_{\ell} \mathbf{h}_{\ell}^H(\mathbf{u}_j) \Theta_{\ell,j} \bar{\mathbf{G}}_{\ell} \right) \mathbf{X}_j \right\|^2 \\ &= \sum_{m=1}^M x_{m,j} \left| \sum_{\ell=1}^L z_{\ell} \mathbf{h}_{\ell}^H(\mathbf{u}_j) \Theta_{\ell,j} \bar{\mathbf{G}}_{\ell}(:, m) \right|^2 \\ &\triangleq \sum_{m=1}^M x_{m,j} \sum_{\ell=1}^L \sum_{\ell'=1}^L (z_{\ell} b_{\ell,j,m}(\mathbf{u}_j)) (z_{\ell'} b_{\ell',j,m}(\mathbf{u}_j))^* \\ &\triangleq \sum_{m=1}^M x_{m,j} \sum_{\ell=1}^L \sum_{\ell'=1}^L z_{\ell} z_{\ell'} B_{\ell,\ell',m,j}(\mathbf{u}_j), \end{aligned} \quad (30)$$

where  $b_{\ell,j,m}(\mathbf{u}_j) \triangleq \mathbf{h}_{\ell}^H(\mathbf{u}_j) \Theta_{\ell,j} \bar{\mathbf{G}}_{\ell}(:, m) \in \mathbb{C}$  and  $B_{\ell,\ell',m,j}(\mathbf{u}_j) \triangleq b_{\ell,j,m}(\mathbf{u}_j) b_{\ell',j,m}^*(\mathbf{u}_j)$ . Accordingly, constraint (28b) can be equivalently rewritten as

$$\begin{aligned} & \bar{P} \sum_{m=1}^M x_{m,j} \sum_{\ell=1}^L \sum_{\ell'=1}^L z_{\ell} z_{\ell'} B_{\ell,\ell',m,j}(\mathbf{u}_j) \geq \gamma_{\text{th},j}, \\ & \forall \mathbf{u}_j \in \mathcal{G}_j, j \in \mathcal{J}. \end{aligned} \quad (31)$$

Note that constraint (31) involves a non-convex triple-product term  $z_{\ell} z_{\ell'} x_{m,j}$ , which couples the binary variables multiplicatively and significantly complicates the optimization. To linearize this constraint, we introduce auxiliary variables:

$$s_{\ell,\ell',m,j} \triangleq z_{\ell} z_{\ell'} x_{m,j}, \quad \forall \ell, \ell' \in \mathcal{L}, m \in \mathcal{M}, j \in \mathcal{J}, \quad (32)$$

and impose the following additional constraints:

$$s_{\ell,\ell',m,j} \in \{0, 1\}, \quad \forall \ell, \ell' \in \mathcal{L}, m \in \mathcal{M}, j \in \mathcal{J}, \quad (33a)$$

$$\begin{aligned} s_{\ell,\ell',m,j} &\leq z_{\ell}, \quad s_{\ell,\ell',m,j} \leq z_{\ell'}, \quad s_{\ell,\ell',m,j} \leq x_{m,j}, \\ \forall \ell, \ell' \in \mathcal{L}, m \in \mathcal{M}, j \in \mathcal{J}, \end{aligned} \quad (33b)$$

$$s_{\ell,\ell',m,j} \geq z_{\ell} + z_{\ell'} + x_{m,j} - 2, \quad \forall \ell, \ell' \in \mathcal{L}, m \in \mathcal{M}, j \in \mathcal{J}. \quad (33c)$$

It can be readily verified that, under the binary constraints (8e) and (8h), as well as the linearization conditions in (33), constraint (31) is equivalent to

$$\begin{aligned} & \bar{P} \sum_{m=1}^M \sum_{\ell=1}^L \sum_{\ell'=1}^L s_{\ell,\ell',m} B_{\ell,\ell',m,j}(\mathbf{u}_j) \geq \gamma_{\text{th},j}, \\ & \forall \mathbf{u}_j \in \mathcal{G}_j, j \in \mathcal{J}. \end{aligned} \quad (34)$$

By replacing constraint (31) with (34) and taking the constraints in (33) into account, we arrive at the following equivalent form of problem (29):

$$\min_{\{x_{m,j}\}, \{z_{\ell}\}, \{s_{\ell,\ell',m,j}\}} c_{\text{MA}} \max_{j \in \mathcal{J}} \left\{ \sum_{m=1}^M x_{m,j} \right\} + \sum_{\ell=1}^L z_{\ell} (c_{\ell} + c_{\text{e}} N_{\ell}) \quad (35a)$$

$$\text{s.t. } (34), (33), (8e) - (8i). \quad (35b)$$

The remaining obstacle to solving this problem is the binary constraints on  $\{x_{m,j}, z_{\ell}, s_{\ell,\ell',m,j}\}$ . To tackle this issue, we employ the same penalty method as in Section III-A. Note that the auxiliary variables  $\{s_{\ell,\ell',m,j}\}$  are coupled with the binary variables  $\{x_{m,j}, z_{\ell}\}$  through the linear inequalities in (33), which constitute a tight convex-hull linearization

of the trilinear product  $s_{\ell,\ell',m,j} = z_\ell z_{\ell'} x_{m,j}$  over the unit hypercube. Specifically, when  $\{x_{m,j}, z_\ell\} \in \{0, 1\}$ , these linear inequalities inherently force  $\{s_{\ell,\ell',m,j}\}$  to take binary values that match the corresponding products. Hence, it suffices to penalize only the binary-constraint violations of  $\{x_{m,j}, z_\ell\}$ .

Accordingly, we relax  $\{x_{m,j}, z_\ell, s_{\ell,\ell',m,j}\}$  from  $\{0, 1\}$  to  $[0, 1]$ . Since the SCA-based penalty construction has been detailed in Section III-A, we omit the derivations and directly apply the same linearization to the quadratic terms  $x_{m,j}^2$  and  $z_\ell^2$ . Let  $\Lambda^{\text{lb},r}(z_\ell) \triangleq (z_\ell^r)^2 + 2z_\ell^r(z_\ell - z_\ell^r)$  denote the first-order Taylor expansion of  $z_\ell^2$  at a given local point  $z_\ell^r$ , and let  $\Pi^{\text{lb},r}(x_{m,j})$  follow the definition in (17). By adding the corresponding penalty terms for  $\{x_{m,j}, z_\ell\}$  to the objective, we obtain the following tractable convex subproblem:

$$\begin{aligned} \min_{\{x_{m,j}\}, \{z_\ell\}, \{s_{\ell,\ell',m,j}\}} \quad & c_{\text{MA}} \max_{j \in \mathcal{J}} \left\{ \sum_{m=1}^M x_{m,j} \right\} + \sum_{\ell=1}^L z_\ell (c_\ell + c_e N_\ell) \\ & + \zeta \sum_{j=1}^J \sum_{m=1}^M (x_{m,j} - \Pi^{\text{lb},r}(x_{m,j})) \\ & + \zeta \sum_{\ell=1}^L (z_\ell - \Lambda^{\text{lb},r}(z_\ell)) \end{aligned} \quad (36a)$$

$$\begin{aligned} \text{s.t.} \quad & 0 \leq x_{m,j} \leq 1, \quad 0 \leq z_\ell \leq 1, \quad 0 \leq s_{\ell,\ell',m,j} \leq 1, \\ & \forall m \in \mathcal{M}, j \in \mathcal{J}, \ell, \ell' \in \mathcal{L}, \end{aligned} \quad (36b)$$

$$(34), (33b), (33c), (8f), (8g), (8i). \quad (36c)$$

Problem (36) is a convex linear program that can be efficiently solved using off-the-shelf solvers (e.g., CVX). Driven by the increasing penalty factor  $\zeta$ , the primary variables  $\{x_{m,j}, z_\ell\}$  converge to binary values, which in turn forces the auxiliary variables  $\{s_{\ell,\ell',m,j}\}$  to satisfy the binary requirement due to the tightness of the inequalities in (33b) and (33c).

### B. Optimizing $\{\Theta_{\ell,j}\}$ for Given $\{x_{m,j}, z_\ell\}$

With the deployment configuration  $\{x_{m,j}, z_\ell\}$  fixed, problem (28) reduces to a feasibility problem regarding the IRS phase-shift variables  $\{\Theta_{\ell,j}\}$ . To improve the convergence behavior, we introduce slack variables  $\{\beta_j\}$  to quantify the per-area SNR margins and reformulate the feasibility task as a margin-maximization problem. These slack variables explicitly represent the SNR margin for each target area  $j$ . Maximizing these margins enlarges the feasible set for the subsequent update of  $\{x_{m,j}, z_\ell\}$ , which helps promote sparser deployments (i.e., fewer deployed MAs/IRSs) in the next iteration. Accordingly, the subproblem for optimizing  $\{\Theta_{\ell,j}\}$  is reformulated as

$$\max_{\{\Theta_{\ell,j}\}, \{\beta_j\}} \sum_{j=1}^J \beta_j \quad (37a)$$

$$\begin{aligned} \text{s.t.} \quad & \bar{P} \left\| \left( \sum_{\ell=1}^L z_\ell \mathbf{h}_\ell^H(\mathbf{u}_j) \Theta_{\ell,j} \bar{\mathbf{G}}_\ell \right) \mathbf{X}_j \right\|^2 \geq \gamma_{\text{th},j} + \beta_j, \\ & \forall \mathbf{u}_j \in \mathcal{G}_j, j \in \mathcal{J}, \end{aligned} \quad (37b)$$

$$(8j). \quad (37c)$$

Problem (37) optimizes the phase shifts only for the deployed IRSs with  $z_\ell = 1$ . Define the deployed-IRS index set  $\mathcal{L}_s \triangleq \{\ell : z_\ell = 1\} \subseteq \mathcal{L}$ , and let  $\mathcal{N}_s$  collect the indices of their reflecting elements, with  $N_s \triangleq |\mathcal{N}_s|$ . Since the quadratic term  $\left\| \left( \sum_{\ell=1}^L z_\ell \mathbf{h}_\ell^H(\mathbf{u}_j) \Theta_{\ell,j} \bar{\mathbf{G}}_\ell \right) \mathbf{X}_j \right\|^2$  has the same structure as in (19), we reuse the compact notations  $\mathbf{v}_j$  and  $\mathbf{R}(\mathbf{u}_j)$ , with dimensions defined over  $\mathcal{L}_s$  and  $\mathcal{N}_s$ . Consequently, problem (37) can be recast as

$$\max_{\{\mathbf{v}_j\}, \{\beta_j\}} \sum_{j=1}^J \beta_j \quad (38a)$$

$$\text{s.t.} \quad \bar{P} \mathbf{v}_j^H \mathbf{R}(\mathbf{u}_j) \mathbf{v}_j \geq \gamma_{\text{th},j} + \beta_j, \forall \mathbf{u}_j \in \mathcal{G}_j, j \in \mathcal{J}, \quad (38b)$$

$$|\mathbf{v}_j|_n = 1, \forall j \in \mathcal{J}, n \in \mathcal{N}_s. \quad (38c)$$

Given that problem (38) shares the same mathematical structure as (20) in Section III-B, we apply the identical SCA and penalty strategies. For brevity, we omit repetitive derivations and directly formulate the convex surrogate subproblem as:

$$\max_{\{\mathbf{v}_j\}, \{\beta_j\}, \{\delta_{j,n}\}} \sum_{j=1}^J \beta_j - \xi \sum_{j=1}^J \sum_{n=1}^{N_s} \delta_{j,n} \quad (39a)$$

$$\text{s.t.} \quad \bar{P} \Xi^{\text{lb},r}(\mathbf{v}_j, \mathbf{u}_j) \geq \gamma_{\text{th},j} + \beta_j, \forall \mathbf{u}_j \in \mathcal{G}_j, j \in \mathcal{J}, \quad (39b)$$

$$|\mathbf{v}_j|_n^2 \leq 1, \forall j \in \mathcal{J}, n \in \mathcal{N}_s, \quad (39c)$$

$$1 - \delta_{j,n} \leq \chi^{\text{lb},r}(|\mathbf{v}_j|_n), \forall j \in \mathcal{J}, n \in \mathcal{N}_s, \quad (39d)$$

where  $\xi$  is a penalty factor, and the linearized terms  $\Xi^{\text{lb},r}(\cdot)$  and  $\chi^{\text{lb},r}(\cdot)$  follow the definitions in Section III-B. Problem (39) is a convex QCQP that can be efficiently solved by existing convex optimization solvers such as CVX.

### C. Overall Algorithm

The proposed algorithm for solving problem (28) adopts a similar double-loop structure to that in Section III. Specifically, the inner loop alternates between optimizing the integer block  $\{x_{m,j}, z_\ell\}$  and the phase-shift block  $\{\Theta_{\ell,j}\}$ , while the penalty factors are updated in the outer loop. Given that the algorithmic framework and convergence properties are analogous to those in the previous section, we omit redundant details and focus solely on the computational complexity, which varies due to the expanded set of variables.

The computational burden is dominated by the resolution of two convex subproblems within each inner iteration. Specifically, solving subproblem (36) entails a complexity of  $\mathcal{O}(C_{\text{dep}} \ln(1/\epsilon))$ , where  $C_{\text{dep}} \triangleq (L^2 M J)^2 (L^2 M J + G)^{1.5}$ , while solving subproblem (39) requires  $\mathcal{O}(C_{\text{ph}} \ln(1/\epsilon))$ , with  $C_{\text{ph}} \triangleq \sqrt{J N_s + G J N_s} (J^2 N_s^2 + J N_s G + G^2)$  [40]. Therefore, the per-iteration complexity of the inner loop is  $\mathcal{O}((C_{\text{dep}} + C_{\text{ph}}) \ln(1/\epsilon))$ .

**Remark 1.** The proposed penalty-based double-loop algorithm readily extends to the **budget-constrained worst-case SNR maximization** counterpart. Specifically, by introducing an auxiliary variable to represent the worst-case SNR and maximizing it subject to a linear cost constraint, the resulting formulation preserves the mathematical structure and non-convex coupling of problem (P1). Consequently, the AO steps

and penalty-based SCA iterations remain effective in handling the binary deployment decisions and non-convex constraints with only minor modifications.

## V. IRS ELEMENT PRUNING FOR FURTHER COST REDUCTION

In the preceding formulation, candidate site  $\ell$  corresponds to an IRS with a predetermined size  $N_\ell$ . Thus, selecting site  $\ell$  (i.e.,  $z_\ell = 1$ ) incurs a fixed element-related cost  $c_e N_\ell$ . This predetermined sizing can be conservative, often yielding an achieved SNR above the target. To exploit this potential margin, we introduce a secondary refinement stage: given the obtained  $\{x_{m,j}, z_\ell, \Theta_{\ell,j}\}$ , we optimize the number of installed elements at each selected IRS to reduce the element-related cost while preserving the SNR guarantees.

### A. Problem Formulation

We introduce a binary installation indicator  $y_{\ell,n} \in \{0, 1\}$  for the  $n$ -th reflecting element at candidate IRS site  $\ell$ , where  $y_{\ell,n} = 1$  indicates that this element is installed and  $y_{\ell,n} = 0$  otherwise. Define  $\mathbf{Y}_\ell = \text{diag}(y_{\ell,1}, \dots, y_{\ell,N_\ell})$ ,  $\forall \ell \in \mathcal{L}$ . Then, the received SNR at location  $\mathbf{u}_j$  in (6) is re-expressed as

$$\gamma_{\mathbf{u}_j} = \bar{P} \left\| \left( \sum_{\ell=1}^L z_\ell \mathbf{h}_\ell^H(\mathbf{u}_j) \mathbf{Y}_\ell \Theta_{\ell,j} \bar{\mathbf{G}}_\ell \right) \mathbf{X}_j \mathbf{w}_{\mathbf{u}_j} \right\|^2. \quad (40)$$

For any given  $\{\mathbf{Y}_\ell\}$ , the MRT beamformer remains optimal. As a result, (40) reduces to

$$\gamma_{\mathbf{u}_j} = \bar{P} \left\| \left( \sum_{\ell=1}^L z_\ell \mathbf{h}_\ell^H(\mathbf{u}_j) \mathbf{Y}_\ell \Theta_{\ell,j} \bar{\mathbf{G}}_\ell \right) \mathbf{X}_j \right\|^2. \quad (41)$$

Moreover, the total infrastructure deployment cost is re-expressed as

$$C_{\text{tot}} = \sum_{\ell=1}^L z_\ell c_e \sum_{n=1}^{N_\ell} y_{\ell,n} + C_{\text{fixed}}, \quad (42)$$

where  $C_{\text{fixed}} \triangleq c_{\text{MA}} \max_{j \in \mathcal{J}} \left\{ \sum_{m=1}^M x_{m,j} \right\} + \sum_{\ell=1}^L z_\ell c_e$ .

We aim to minimize the element-related deployment cost by optimizing the installation indicators  $\{y_{\ell,n}\}$ , while maintaining the SNR requirements. This yields the following problem:

$$(P3) : \min_{\{y_{\ell,n}\}} \sum_{\ell=1}^L z_\ell c_e \sum_{n=1}^{N_\ell} y_{\ell,n} + C_{\text{fixed}} \quad (43a)$$

$$\text{s.t. } \bar{P} \left\| \left( \sum_{\ell=1}^L z_\ell \mathbf{h}_\ell^H(\mathbf{u}_j) \mathbf{Y}_\ell \Theta_{\ell,j} \bar{\mathbf{G}}_\ell \right) \mathbf{X}_j \right\|^2 \geq \gamma_{\text{th},j}, \quad \forall u_j \in \mathcal{G}_j, j \in \mathcal{J}, \quad (43b)$$

$$\mathbf{Y}_\ell = \text{diag}(y_{\ell,1}, \dots, y_{\ell,N_\ell}), \quad \forall \ell \in \mathcal{L}, \quad (43c)$$

$$y_{\ell,n} \in \{0, 1\}, \quad \forall \ell \in \mathcal{L}, n \in \mathcal{N}_\ell, \quad (43d)$$

$$y_{\ell,n} \leq z_\ell, \quad \forall \ell \in \mathcal{L}, n \in \mathcal{N}_\ell, \quad (43e)$$

where constraint (43e) implies that  $y_{\ell,n} = 0$  whenever  $z_\ell = 0$ . Problem (P3) is a pure binary optimization problem. The binary constraints render it combinatorial, and the quadratic SNR constraints further make the feasible set non-convex, which together make (P3) challenging to solve globally.

### B. Proposed Algorithm for Problem (P3)

To efficiently solve (P3), we first reformulate the quadratic constraints into a more tractable form. Let  $\mathbf{f}_{\ell,j,n}^T$  denote the  $n$ -th row of the effective channel matrix  $\mathbf{F}_{\ell,j} \triangleq \Theta_{\ell,j} \bar{\mathbf{G}}_\ell \mathbf{X}_j \in \mathbb{C}^{N_\ell \times M}$ . By defining an equivalent aggregated channel vector  $\mathbf{c}_{\ell,j,n}^T(\mathbf{u}_j) \triangleq [\mathbf{h}_\ell^H(\mathbf{u}_j)]_n \mathbf{f}_{\ell,j,n}^T$ , the beamforming gain term in (43b) can be expanded as

$$\begin{aligned} \gamma_{\mathbf{u}_j} &= \bar{P} \left\| \sum_{\ell=1}^L \sum_{n=1}^{N_\ell} z_\ell y_{\ell,n} [\mathbf{h}_\ell^H(\mathbf{u}_j)]_n \mathbf{f}_{\ell,j,n}^T \right\|^2 \\ &= \bar{P} \left\| \sum_{\ell=1}^L \sum_{n=1}^{N_\ell} z_\ell y_{\ell,n} \mathbf{c}_{\ell,j,n}^T(\mathbf{u}_j) \right\|^2, \\ &= \bar{P} \sum_{\ell,n} \sum_{\ell',n'} z_\ell z_{\ell'} y_{\ell,n} y_{\ell',n'} \mathbf{c}_{\ell,j,n}^T(\mathbf{u}_j) \mathbf{c}_{\ell',j,n'}^*(\mathbf{u}_j). \end{aligned} \quad (44)$$

For compact representation, we stack all binary variables  $\{y_{\ell,n}\}$  into a single vector  $\mathbf{y} \triangleq [\mathbf{y}_1^T, \mathbf{y}_2^T, \dots, \mathbf{y}_L^T]^T \in \{0, 1\}^{N \times 1}$ . We then construct a Hermitian matrix  $\mathbf{Q}(\mathbf{u}_j) \in \mathbb{C}^{N \times N}$ , where the entry corresponding to the indices of  $(\ell_u, n_u)$  and  $(\ell_v, n_v)$  is given by

$$[\mathbf{Q}(\mathbf{u}_j)]_{u,v} = z_{\ell_u} z_{\ell_v} \mathbf{c}_{\ell_u,j,n_u}^T(\mathbf{u}_j) \mathbf{c}_{\ell_v,j,n_v}^*(\mathbf{u}_j). \quad (45)$$

Accordingly,  $\gamma_{\mathbf{u}_j}$  is recast as the quadratic form  $\gamma_{\mathbf{u}_j} = \bar{P} \mathbf{y}^H \mathbf{Q}(\mathbf{u}_j) \mathbf{y}$ . Problem (P3) is equivalently transformed into

$$\min_{\{y_{\ell,n}\}} \sum_{\ell=1}^L z_\ell c_e \sum_{n=1}^{N_\ell} y_{\ell,n} + C_{\text{fixed}} \quad (46a)$$

$$\text{s.t. } \bar{P} \mathbf{y}^H \mathbf{Q}(\mathbf{u}_j) \mathbf{y} \geq \gamma_{\text{th},j}, \quad \forall u_j \in \mathcal{G}_j, j \in \mathcal{J}, \quad (46b)$$

$$(43d), (43e). \quad (46c)$$

To address the non-convex constraint (46b), we adopt the SCA method. Specifically, the quadratic term  $\mathbf{y}^H \mathbf{Q}(\mathbf{u}_j) \mathbf{y}$  is replaced by its first-order Taylor expansion-based lower bound at a given local point  $\mathbf{y}^r$  in the  $r$ -th iteration. As a result, problem (46) is approximated as

$$\min_{\{y_{\ell,n}\}} \sum_{\ell=1}^L z_\ell c_e \sum_{n=1}^{N_\ell} y_{\ell,n} + C_{\text{fixed}} \quad (47a)$$

$$\text{s.t. } \bar{P} \left( 2\Re \left\{ (\mathbf{y}^r)^H \mathbf{Q}(\mathbf{u}_j) \mathbf{y} \right\} - (\mathbf{y}^r)^H \mathbf{Q}(\mathbf{u}_j) \mathbf{y}^r \right) \geq \gamma_{\text{th},j},$$

$$\forall u_j \in \mathcal{G}_j, j \in \mathcal{J}, \quad (47b)$$

$$(43d), (43e). \quad (47c)$$

Problem (47) is a standard 0-1 integer linear program. To avoid combinatorial search, we relax the binary variables  $\{y_{\ell,n}\}$  from  $\{0, 1\}$  to  $[0, 1]$  and add an integrality-violation penalty to the objective, thereby transforming problem (47) into the following convex linear program:

$$\min_{\{y_{\ell,n}\}} \sum_{\ell=1}^L z_\ell c_e \sum_{n=1}^{N_\ell} y_{\ell,n} + C_{\text{fixed}} + \nu \sum_{\ell=1}^L \sum_{n=1}^{N_\ell} (y_{\ell,n} - \Upsilon^{\text{lb},r}(y_{\ell,n})) \quad (48a)$$

$$\text{s.t. } 0 \leq y_{\ell,n} \leq 1, \quad \forall \ell \in \mathcal{L}, n \in \mathcal{N}_\ell, \quad (48b)$$

$$(47b), (43e), \quad (48c)$$

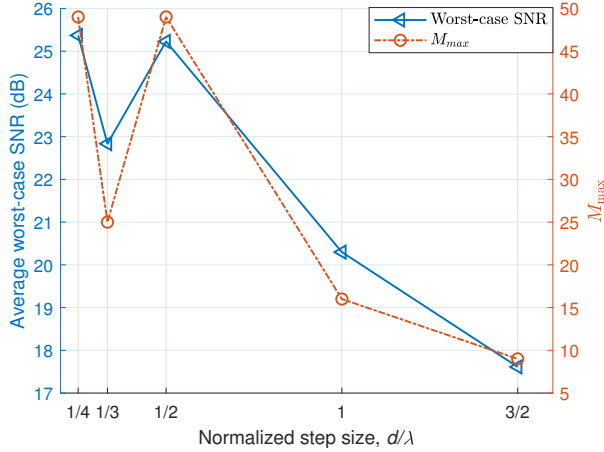


Fig. 2. Average worst-case SNR versus normalized step size.

where  $\nu \geq 0$  is a penalty factor, and  $\Upsilon^{\text{lb},r}(y_{\ell,n}) \triangleq \left(y_{\ell,n}^r\right)^2 + 2y_{\ell,n}^r(y_{\ell,n} - y_{\ell,n}^r)$  represents the first-order Taylor expansion of  $y_{\ell,n}^2$  at a given local point  $y_{\ell,n}^r$ . Problem (48) can be efficiently solved using convex optimization tools such as CVX, with a complexity of  $\mathcal{O}((G + 2N)^{1.5}N^2 \ln(1/\epsilon))$  [40]. The final binary solution is obtained by iteratively solving problem (48) with a progressively increasing penalty factor  $\nu$ .

## VI. SIMULATION RESULTS

This section evaluates the proposed designs through numerical simulations. The carrier frequency is 3 GHz ( $\lambda = 0.1$  m) [25], giving a reference channel gain at 1 m of  $C_0 = (\lambda/4\pi)^2$ . We consider  $L = 5$  candidate IRS sites with coordinates (in m):  $[5, 0, 12]^T$ ,  $[0, 12, 5]^T$ ,  $[0, -12, 5]^T$ ,  $[10, 25, 5]^T$ , and  $[10, -25, 5]^T$ . The first site hosts a horizontally oriented IRS facing downwards (e.g., on an uncrewed aerial vehicle or a ceiling), while the others are vertically oriented (e.g., on building facades or walls). Each IRS is a uniform planar array with half-wavelength spacing. Target areas are  $5 \text{ m} \times 5 \text{ m}$  disjoint squares, randomly placed within  $x \in [50, 70] \text{ m}$ ,  $y \in [-40, 40] \text{ m}$ ,  $z = 0 \text{ m}$ , and sampled at 1-m intervals. Cost parameters are normalized to the per-element cost  $c_e = 1$ . The fixed deployment costs for the five sites are given by  $c_\ell = \{30, 20, 20, 10, 10\}$  for  $\ell = 1, \dots, 5$ . Default simulation parameters are:  $P = 20$  dBm,  $\sigma^2 = -90$  dBm,  $J = 2$ ,  $c_{\text{MA}} = 30$ ,  $A = 3\lambda$ ,  $D = \lambda/2$  [22],  $d = \lambda/2$ , and  $N_\ell = 50$  potential elements per IRS (arranged  $5 \times 10$ ). A uniform SNR target  $\gamma = 10$  dB is imposed for all  $\mathbf{u}_j \in \mathcal{G}_j, j \in \mathcal{J}$ .

### A. Feasibility Check via Worst-Case SNR Maximization

In this subsection, we evaluate the feasibility limit under the full-configuration scenario. With identical target SNRs, maximizing  $\eta$  in the feasibility check problem (P2) is mathematically equivalent to maximizing the worst-case SNR across all the target areas. We therefore use the maximum achievable worst-case SNR as our primary metric. This value provides a quantitative feasibility boundary: any target SNR below it is feasible, offering more information than a binary feasible-infeasible check.

Fig. 2 shows the average worst-case SNR (left axis) and the maximum allowable number of MAs,  $M_{\max}$  (right axis), versus the normalized grid step size  $d/\lambda$ . The worst-case SNR closely tracks  $M_{\max}$ , which is determined by the interplay between the grid step size  $d$  and the minimum inter-MA spacing requirement  $D$ . In particular,  $d = \lambda/4$  and  $d = \lambda/2$  both enable near-optimal packing ( $M_{\max} = 49$ ), yielding the highest SNR of about 25 dB. Although  $d = \lambda/4$  provides slightly more spatial flexibility, its gain over  $d = \lambda/2$  is marginal because  $M_{\max}$  is saturated in both cases. By contrast, a pronounced dip occurs at  $d = \lambda/3$ , where grid-spacing misalignment limits packing ( $M_{\max} = 25$ ) and reduces the resulting SNR to approximately 23 dB, indicating that a finer grid does not necessarily improve performance. For coarse grids ( $d > \lambda/2$ ),  $M_{\max}$  decreases monotonically, leading to a substantial SNR loss. Overall,  $d = \lambda/2$  offers a good trade-off between performance and computational complexity.

### B. Deployment Cost Minimization Under SNR Constraints

In this subsection, we assess the cost-effectiveness of the proposed designs by comparing the following schemes. For all schemes, the transmit beamforming is chosen as MRT based on the end-to-end effective channels.

- **Proposed joint MA-IRS:** The approach in Section IV, which jointly optimizes the MA placement, IRS site selection, and IRS phase shifts, assuming full-size IRS panels (i.e.,  $N_\ell$  elements) at the selected sites.
- **Proposed element pruning:** The method in Section V that further optimizes the number of installed IRS elements based on the joint MA-IRS solution.
- **Per-area union:** A baseline that performs independent optimization for each target area, with the deployment cost computed from the union of selected IRS sites and the maximum MA number over all areas.
- **MA-(all IRS):** A benchmark with all candidate IRSs deployed, i.e.,  $z_\ell = 1, \forall \ell \in \mathcal{L}$ , where only the MA placement and IRS phase shifts are optimized.
- **FPA-IRS:** An FPA benchmark that deploys antennas at all feasible grid points (subject to the minimum spacing constraint) and optimizes the IRS site selection and phase shifts. The unit cost ratio is defined as  $\kappa \triangleq c_{\text{FPA}}/c_{\text{MA}}$  and is set to  $\kappa = 1/3$  unless otherwise specified.

1) *Impact of Unit Cost of MAs:* Fig. 3 examines the impact of the MA unit cost  $c_{\text{MA}}$  on the deployment performance. In Fig. 3(a), the average normalized deployment cost increases with  $c_{\text{MA}}$  for all schemes, with the FPA-IRS scheme rising the fastest because its fully populated FPA array incurs a large fixed antenna cost even when  $\kappa = 1/3$ . The MA-(all IRS) benchmark remains costly yet relatively insensitive to  $c_{\text{MA}}$  because deploying all 5 IRSs dominates the cost. The per-area union baseline performs better but still incurs higher costs than the proposed methods due to the lack of inter-area resource sharing. By contrast, the proposed joint MA-IRS scheme achieves substantial cost savings by jointly optimizing MA placement and selecting only the necessary IRSs. As highlighted in the zoomed-in view, the proposed element pruning scheme further reduces the cost by pruning

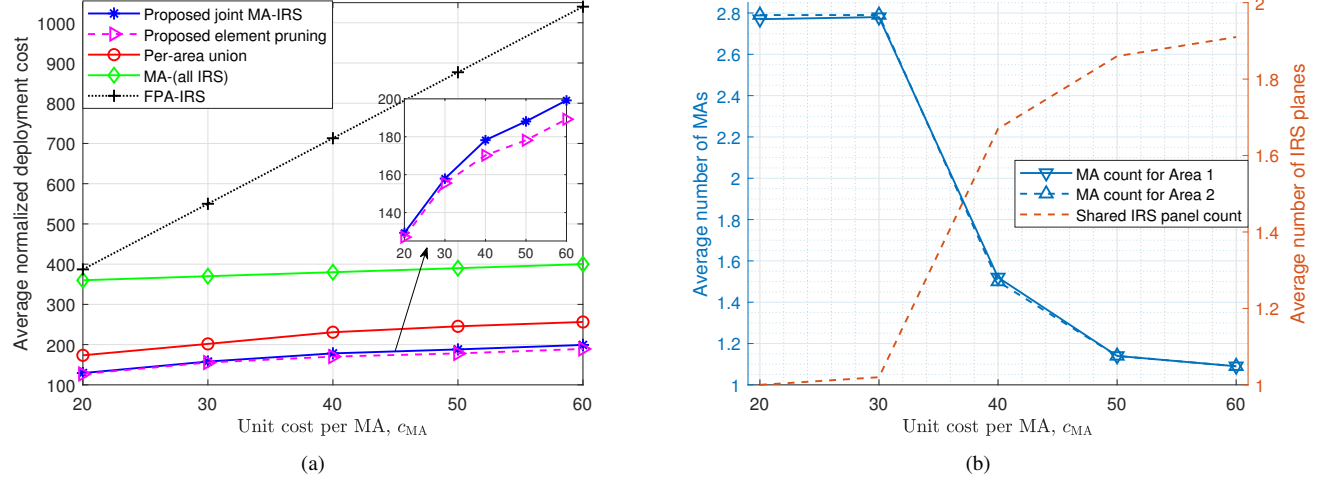


Fig. 3. Impact of the MA unit cost  $c_{MA}$ . (a) Average normalized deployment cost. (b) Average MA count per area and shared IRS panel count under the proposed joint MA-IRS design.

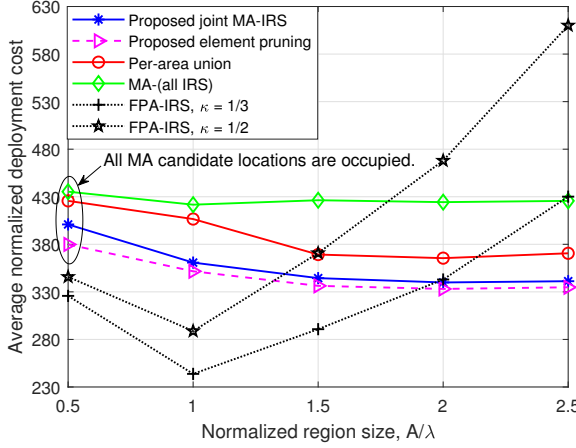


Fig. 4. Average normalized deployment cost versus normalized region size.

redundant elements from the selected IRSs, validating the benefit of the second-stage refinement.

To provide deeper insights into the cost-saving mechanism of the proposed joint MA-IRS scheme, Fig. 3(b) plots the average number of deployed MAs and shared IRS panels versus  $c_{MA}$ . A clear resource trade-off is observed. In the low-cost regime where  $c_{MA} \leq 30$ , the system favors deploying more MAs, approximately 2.8 per area, while activating only a minimal number of IRSs, around 1. This occurs because MAs provide high beamforming gain at a low cost, which reduces the reliance on IRSs. However, as  $c_{MA}$  increases beyond 30, the number of MAs drops sharply to nearly 1. Meanwhile, the number of deployed IRSs increases to compensate for the reduced active gain. This demonstrates the capability of the algorithm to adaptively substitute expensive active resources with more cost-effective passive resources to minimize the total deployment cost.

2) *Impact of Normalized Region Size:* Fig. 4 illustrates the deployment cost versus the normalized region size  $A/\lambda$ , where the target SNR is set to  $\gamma = 15$  dB. Two notable phenomena regarding the cost behaviors are observed. First,

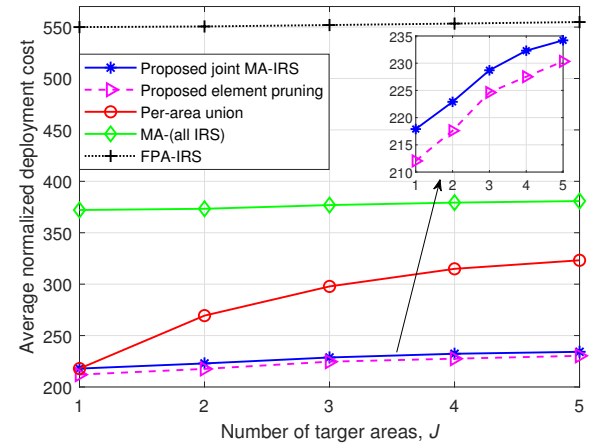


Fig. 5. Average normalized deployment cost versus number of target areas.

the cost of the FPA-IRS scheme follows a non-monotonic U-shaped trend, which decreases initially before escalating rapidly. The initial decrease occurs because the enhanced array gain from a slightly larger aperture allows the system to deactivate expensive IRSs. The resulting savings outweigh the cost of adding a few cheap FPA elements. However, as  $A$  grows further, the cost rises sharply since the number of fixed antennas grows quadratically. Second, the proposed joint MA-IRS scheme is not invariably superior to the FPA benchmarks, especially in compact regions. At  $A = 0.5\lambda$ , the MA system is saturated and physically degenerates into a fully populated array, thus incurring a higher cost due to the unit cost premium of MAs. Even at moderate sizes, the limited spatial degrees of freedom prevent the MA position optimization from sufficiently reducing the RF chain count to offset this premium. Consequently, the FPA architecture is more cost-effective for compact regions, while the proposed MA scheme is superior for realizing large-aperture transmitters by exploiting spatial diversity to minimize hardware usage.

3) *Impact of Number of Target Areas:* Fig. 5 depicts the average normalized deployment cost versus the number of

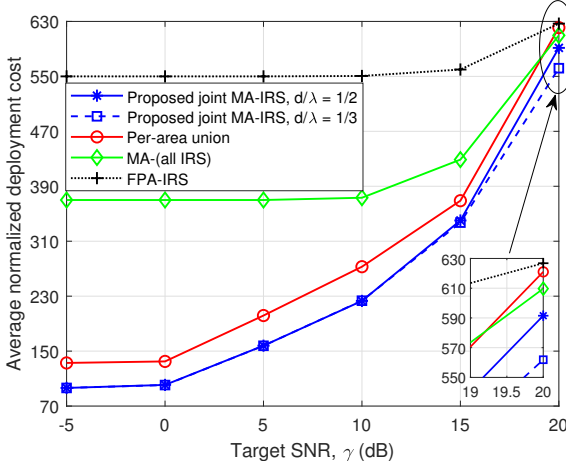


Fig. 6. Average normalized deployment cost versus target SNR.

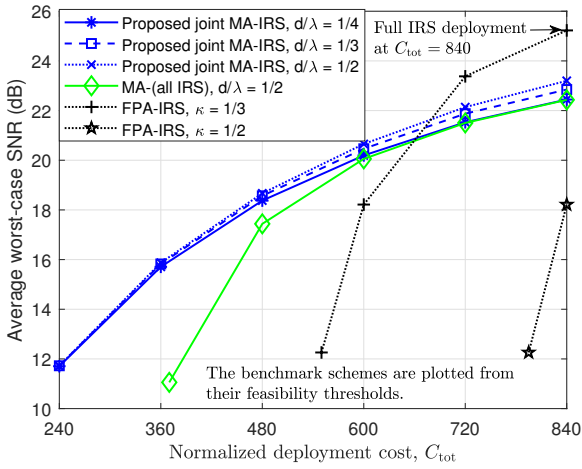


Fig. 7. Average worst-case SNR versus normalized deployment cost.

target areas  $J$ . A significant performance gap emerges between the proposed joint MA-IRS scheme and the per-area union benchmark as  $J$  increases. At  $J = 1$ , the two schemes yield identical costs since the resource union for a single area is trivial. However, as  $J$  grows, the cost of the per-area union scheme rises rapidly. This is because it optimizes resources for each area independently and aggregates them without exploiting potential overlaps. In contrast, the cost of the proposed joint MA-IRS scheme increases only marginally. This highlights the advantage of resource reuse. By identifying a minimum common set of hardware reconfigurable to serve different areas, the proposed joint MA-IRS scheme avoids the redundancy of dedicated deployments. Meanwhile, the FPA-IRS and MA-(all IRS) schemes incur much higher costs due to the deployment of excessive fixed resources which are insensitive to the actual coverage requirements. Finally, as shown in the zoomed-in view, the proposed element pruning scheme consistently achieves the lowest cost by eliminating redundant elements from the selected IRSs.

4) *Impact of Target SNR:* Fig. 6 presents the average normalized deployment cost versus the target SNR  $\gamma$ . As anticipated, the deployment costs for all schemes escalate as  $\gamma$  increases since more active MAs and passive IRSs are

required to meet the stricter QoS requirements. Throughout the plotted range, the proposed joint MA-IRS scheme consistently achieves the lowest cost among all considered benchmarks.

Two interesting phenomena are observed in the high-SNR regime at  $\gamma = 20$  dB. First, the cost gap between the proposed joint MA-IRS scheme and the MA-(all IRS) benchmark becomes much smaller. This is because the stringent SNR target forces the proposed algorithm to activate most candidate IRSs. As the active-IRS set approaches the full set, the cost-saving potential from IRS selection largely vanishes, and the proposed scheme effectively converges to the all-IRS benchmark. Second, the proposed scheme with  $d/\lambda = 1/3$  achieves a lower cost than that with  $d/\lambda = 1/2$ . Although this seems counter-intuitive given the smaller allowable MA count for  $d/\lambda = 1/3$  in Fig. 2 (i.e.,  $M_{\max} = 25$  versus 49), the key is that at  $\gamma = 20$  dB the required MA number remains below  $M_{\max}$  for  $d/\lambda = 1/3$ . In this non-saturated regime, the  $d/\lambda = 1/3$  grid provides finer spatial resolution than  $d/\lambda = 1/2$ , enabling more effective exploitation of small-scale fading and higher end-to-end channel gains. Consequently, the target SNR can be met with lower hardware expenditure. By contrast, in the low-SNR regime, the hardware requirement is already minimal, and the additional spatial gain from a finer grid is insufficient to reduce the discrete integer numbers of deployed elements, leading to negligible cost differences between the two step sizes.

### C. Worst-Case SNR Maximization Under a Cost Budget

Fig. 7 depicts the average worst-case SNR versus the normalized deployment cost budget, highlighting the trade-off between MA flexibility and the low unit cost of FPAs.

In the low-to-medium cost regime, the proposed joint MA-IRS scheme consistently achieves a higher worst-case SNR than all benchmarks under the same budget. In particular, the FPA-IRS benchmark is infeasible when  $C_{\text{tot}} < 550$  for  $\kappa = 1/3$  and when  $C_{\text{tot}} < 795$  for  $\kappa = 1/2$ , indicating a high feasibility threshold under the adopted FPA deployment setting. By contrast, MA-based designs exploit position optimization to harvest spatial diversity with only a few active RF chains, making them attractive under tight budget constraints.

In the high-cost regime, relative performance depends heavily on the unit cost ratio  $\kappa$ . When FPAs are significantly cheaper with  $\kappa = 1/3$ , the FPA-IRS benchmark reaches approximately 25 dB at  $C_{\text{tot}} = 840$  by enabling full deployment. This allows the system to approach the aperture-limited performance ceiling. In contrast, the proposed MA-IRS scheme optimizes both MAs and IRSs under the same budget constraint. Due to the higher unit cost of MAs, the restricted budget limits the number of deployable MAs and IRSs compared to the fully populated FPA benchmark. Consequently, this trade-off may yield a slightly lower SNR despite the benefits of position optimization. However, with moderately expensive FPAs ( $\kappa = 1/2$ ), the MA scheme retains its superiority even at high budgets. Furthermore, among the proposed schemes, the grid with  $d/\lambda = 1/3$  outperforms  $d/\lambda = 1/2$ . This confirms that in the non-saturated regime where the number of MAs is far below  $M_{\max}$ , a finer grid resolution provides higher spatial degrees of freedom to improve beamforming gain.

## VII. CONCLUSION

In this paper, we proposed a two-scale spatial deployment framework where macroscopic IRS site selection shapes the propagation geometry and microscopic MA repositioning exploits local channel variations. We formulated a joint optimization problem to minimize the total hardware cost by coordinating IRS site selection, MA positioning, and beamforming design, subject to specific QoS requirements for multiple target areas. A penalty-based AO algorithm was first devised to solve the feasibility and cost minimization problems, followed by a secondary element refinement stage to strictly eliminate hardware redundancy. Simulation results validated the effectiveness of the proposed designs and provided critical engineering insights into MA grid discretization, as well as guidelines for selecting between MA and fully populated FPA architectures depending on placement aperture sizes for cost minimization, and budget levels for worst-case SNR maximization.

## REFERENCES

- [1] A. J. Paulraj, D. A. Gore, R. U. Nabar, and H. Bolcskei, "An overview of MIMO communications-a key to gigabit wireless," *Proc. IEEE*, vol. 92, no. 2, pp. 198–218, Feb. 2004.
- [2] E. G. Larsson, O. Edfors, F. Tufvesson, and T. L. Marzetta, "Massive MIMO for next generation wireless systems," *IEEE Commun. Mag.*, vol. 52, no. 2, pp. 186–195, Feb. 2014.
- [3] M. Z. Chowdhury *et al.*, "6G wireless communication systems: Applications, requirements, technologies, challenges, and research directions," *IEEE Open J. Commun. Soc.*, vol. 1, pp. 957–975, Jul. 2020.
- [4] Q. Wu and R. Zhang, "Intelligent reflecting surface enhanced wireless network via joint active and passive beamforming," *IEEE Trans. Wireless Commun.*, vol. 18, no. 11, pp. 5394–5409, Nov. 2019.
- [5] Q. Wu, G. Chen, Q. Peng *et al.*, "Intelligent reflecting surfaces for wireless networks: Deployment architectures, key solutions, and field trials," *IEEE Wireless Commun.*, 2025, early access, doi: 10.1109/WC.2025.92500020.
- [6] Q. Wu and R. Zhang, "Beamforming optimization for wireless network aided by intelligent reflecting surface with discrete phase shifts," *IEEE Trans. Commun.*, vol. 68, no. 3, pp. 1838–1851, Mar. 2020.
- [7] M. Cui, G. Zhang, and R. Zhang, "Secure wireless communication via intelligent reflecting surface," *IEEE Wireless Commun. Lett.*, vol. 8, no. 5, pp. 1410–1414, Oct. 2019.
- [8] X. Guan, Q. Wu, and R. Zhang, "Intelligent reflecting surface assisted secrecy communication: Is artificial noise helpful or not?" *IEEE Wireless Commun. Lett.*, vol. 9, no. 6, pp. 778–782, Jun. 2020.
- [9] W. Mei, B. Zheng, C. You *et al.*, "Intelligent reflecting surface-aided wireless networks: From single-reflection to multireflection design and optimization," *Proc. IEEE*, vol. 110, no. 9, pp. 1380–1400, Sep. 2022.
- [10] Y. Gao, Q. Wu, G. Zhang *et al.*, "Beamforming optimization for active intelligent reflecting surface-aided SWIPT," *IEEE Trans. Wireless Commun.*, vol. 22, no. 1, pp. 362–378, Jan. 2023.
- [11] Q. Peng, Q. Wu, G. Chen, W. Chen, S. Ma, S. Shen, and R. Zhang, "Rotatable IRS aided wireless communication," 2025, *arXiv: 2511.10006*. [Online]. Available: <https://arxiv.org/abs/2511.10006>
- [12] Q. Peng, Q. Wu, G. Chen, W. Chen, S. Shen, and S. Ma, "Cooperative rotatable IRSs for wireless communications: Joint beamforming and orientation optimization," 2025, *arXiv: 2512.14037*. [Online]. Available: <https://arxiv.org/abs/2512.14037>
- [13] H. Lu, Y. Zeng, S. Jin, and R. Zhang, "Aerial intelligent reflecting surface: Joint placement and passive beamforming design with 3D beam flattening," *IEEE Trans. Wireless Commun.*, vol. 20, no. 7, pp. 4128–4143, Jul. 2021.
- [14] G. Chen, Q. Wu, C. Wu *et al.*, "Static IRS meets distributed MIMO: A new architecture for dynamic beamforming," *IEEE Wireless Commun. Lett.*, vol. 12, no. 11, pp. 1866–1870, Nov. 2023.
- [15] J. Feng, B. Zheng, C. You *et al.*, "Joint passive beamforming and deployment design for dual distributed-IRS aided communication," *IEEE Trans. Veh. Technol.*, vol. 72, no. 10, pp. 13758–13763, Oct. 2023.
- [16] H. Al-Tous and O. Tirkkonen, "Coverage area optimized static reflecting surfaces," *IEEE Trans. Wireless Commun.*, vol. 23, no. 8, pp. 9375–9388, Aug. 2024.
- [17] W. Mei and R. Zhang, "Joint base station and IRS deployment for enhancing network coverage: A graph-based modeling and optimization approach," *IEEE Trans. Wireless Commun.*, vol. 22, no. 11, pp. 8200–8213, Nov. 2023.
- [18] M. Fu, L. Zhu, and R. Zhang, "Multi-IRS enhanced wireless coverage: Deployment optimization based on large-scale channel knowledge," *IEEE Trans. Wireless Commun.*, vol. 24, no. 11, pp. 9069–9084, Nov. 2025.
- [19] L. Zhu, W. Ma, and R. Zhang, "Movable antennas for wireless communication: Opportunities and challenges," *IEEE Commun. Mag.*, vol. 62, no. 6, pp. 114–120, Jun. 2024.
- [20] —, "Modeling and performance analysis for movable antenna enabled wireless communications," *IEEE Trans. Wireless Commun.*, vol. 23, no. 6, pp. 6234–6250, Jun. 2024.
- [21] K.-K. Wong *et al.*, "Fluid antenna systems," *IEEE Trans. Wireless Commun.*, vol. 20, no. 3, pp. 1950–1962, Mar. 2021.
- [22] W. Ma, L. Zhu, and R. Zhang, "MIMO capacity characterization for movable antenna systems," *IEEE Trans. Wireless Commun.*, vol. 23, no. 4, pp. 3392–3407, Apr. 2024.
- [23] L. Zhu, W. Ma, B. Ning, and R. Zhang, "Movable-antenna enhanced multiuser communication via antenna position optimization," *IEEE Trans. Wireless Commun.*, vol. 23, no. 7, pp. 7214–7229, Jul. 2024.
- [24] H. Qin, W. Chen, Z. Li *et al.*, "Antenna positioning and beamforming design for fluid antenna-assisted multi-user downlink communications," *IEEE Wireless Commun. Lett.*, vol. 13, no. 4, pp. 1073–1077, Apr. 2024.
- [25] Z. Xiao, X. Pi, L. Zhu, X.-G. Xia, and R. Zhang, "Multiuser communications with movable-antenna base station: Joint antenna positioning, receive combining, and power control," *IEEE Trans. Wireless Commun.*, vol. 23, no. 12, pp. 19744–19759, Dec. 2024.
- [26] Z. Zheng, Q. Wu, W. Chen, and G. Hu, "Two-timescale design for movable antennas enabled multiuser MIMO systems," *IEEE Trans. Wireless Commun.*, 2025, early access, doi: 10.1109/TCOMM.2025.3585515.
- [27] H. Wang, Q. Wu, and W. Chen, "Movable antenna enabled interference network: Joint antenna position and beamforming design," *IEEE Wireless Commun. Lett.*, vol. 13, no. 9, pp. 2517–2521, Sep. 2024.
- [28] Y. Gao, Q. Wu, and W. Chen, "Joint transmitter and receiver design for movable antenna enhanced multicast communications," *IEEE Trans. Wireless Commun.*, vol. 23, no. 12, pp. 18186–18200, Dec. 2024.
- [29] G. Hu, Q. Wu, K. Xu, J. Si, and N. Al-Dahir, "Secure wireless communication via movable-antenna array," *IEEE Signal Process. Lett.*, vol. 31, pp. 516–520, Jan. 2024.
- [30] X. Wei, W. Mei, D. Wang *et al.*, "Joint beamforming and antenna position optimization for movable antenna-assisted spectrum sharing," *IEEE Wireless Commun. Lett.*, vol. 13, no. 9, pp. 2502–2506, Sep. 2024.
- [31] Y. Gao, Q. Wu, and W. Chen, "Movable antennas enabled wireless-powered NOMA: Continuous and discrete positioning designs," *IEEE Trans. Wireless Commun.*, 2025, early access, doi: 10.1109/TWC.2025.3629352.
- [32] L. Zhu, W. Ma, W. Mei *et al.*, "A tutorial on movable antennas for wireless networks," *IEEE Commun. Surv. Tutor.*, 2025, early access, doi: 10.1109/COMST.2025.3546373.
- [33] Q. Wu, Z. Zheng, Y. Gao, W. Mei, X. Wei, W. Chen, and B. Ning, "Integrating movable antennas and intelligent reflecting surfaces (MA-IRS): Fundamentals, practical solutions, and isac," *IEEE Wireless Commun.*, 2025, early access, doi: 10.1109/MWC.2025.3623970.
- [34] F. R. Ghadi, K.-K. Wong, W. K. New, H. Xu, R. Murch, and Y. Zhang, "On performance of RIS-aided fluid antenna systems," *IEEE Wireless Commun. Lett.*, vol. 13, no. 8, pp. 2175–2179, Aug. 2024.
- [35] Y. Sun, H. Xu, B. Ning *et al.*, "Sum-rate optimization for RIS-aided multiuser communications with movable antennas," *IEEE Wireless Commun. Lett.*, vol. 14, no. 2, pp. 450–454, Feb. 2025.
- [36] J. Yao, L. Zhou, T. Wu *et al.*, "FAS vs. ARIS: Which is more important for FAS-ARIS communication systems?" *IEEE Trans. Wireless Commun.*, 2025, early access, doi: 10.1109/TWC.2025.3594617.
- [37] X. Wei, W. Mei, Q. Wu *et al.*, "Movable antennas meet intelligent reflecting surface: Friends or foes?" *IEEE Trans. Commun.*, 2025, early access, doi: 10.1109/TCOMM.2025.3588579.
- [38] F. R. Ghadi, K.-K. Wong, M. Kaveh *et al.*, "Secrecy performance analysis of RIS-aided fluid antenna systems," in *Proc. IEEE WCNC*, Milan, Italy, Mar. 2025, pp. 1–6.
- [39] Y. Gao, Q. Wu, W. Mei *et al.*, "Integrating movable antennas and intelligent reflecting surfaces for coverage enhancement," *IEEE Trans. Wireless Commun.*, 2025, early access, doi: 10.1109/TWC.2025.3623474.
- [40] K. Wang, A. M. So, T. Chang *et al.*, "Outage constrained robust transmit optimization for multiuser MISO downlinks: Tractable approximations by conic optimization," *IEEE Trans. Signal Process.*, vol. 62, no. 21, pp. 5690–5705, Nov. 2014.